Moderate Elevation of Homocysteine Induces Endothelial Dysfunction through Adaptive UPR Activation and Metabolic Rewiring

Barun Chatterjee , Fabeha Fatima , Surabhi Seth , Soumya Sinha Roy *

Posted Date: 5 September 2023

doi: 10.20944/preprints202309.0215.v1

Keywords: Homocysteine; endothelial cell; angiogenesis; zebrafish; ER stress; actin cytoskeleton; mitochondria; glycolysis; TCA cycle

Article

Moderate Elevation of Homocysteine Induces Endothelial Dysfunction through Adaptive UPR Activation and Metabolic Rewiring

Barun Chatterjee [1,2], Fabeha Fatima [1], Surabhi Seth [1,2] and Soumya Sinha Roy [1,2,*]

[1] CSIR - Institute of Genomics & Integrative Biology, New Delhi 110025, India.
[2] Academy of Scientific & Innovative Research, Ghaziabad - 201002, India.
* Correspondence: CSIR-Institute of Genomics & Integrative Biology, Mathura Road, Sukhdev Vihar, New Delhi, 110020, India, Tel. 91-11-29879 107, Fax: 91-11-27667 471, E-mail soumya.roy@igib.res.in

Abstract: Elevation of the intermediate amino acid metabolite Homocysteine (Hcy) causes Hyperhomocysteinemia (HHcy), a metabolic disorder frequently associated with mutations in the methionine-cysteine metabolic cycle as well as with nutritional deficiency and aging. Previous literature suggest that HHcy is a strong risk factor for cardiovascular diseases. Severe HHcy is well established to correlate with vascular pathologies primarily via endothelial cell death. Though moderate HHcy is more prevalent and associated with an increased risk of cardiovascular abnormalities in later part of life, its precise role in endothelial physiology is largely unknown. In this study, we report that moderate elevation of Hcy causes endothelial dysfunction through impairment of their migration and proliferation. We established that unlike severe elevation of Hcy, moderate HHcy is not associated with suppressed endothelial VEGF/VEGFR signaling and oxidative stress induction. We further showed that moderate HHcy induces a sub-lethal ER stress that causes defective endothelial migration through abnormal actin cytoskeletal remodeling. We also found that sub-lethal increase of Hcy causes endothelial proliferation defect by suppressing mitochondrial respiration and concomitantly increases glycolysis to compensate the consequential ATP loss and maintain overall energy homeostasis. Finally, analyzing an available microarray dataset, we confirmed that these hallmarks of moderate HHcy are conserved in adult endothelial cells as well. Thus, we identified adaptive UPR and metabolic rewiring as two key mechanistic signatures in moderate HHcy-associated endothelial dysfunction. As HHcy is clinically associated with enhanced vascular inflammation and hypercoagulability, identifying these mechanistic pathways may serve as future targets to regulate endothelial function and health.

Keywords: Homocysteine; endothelial cell; angiogenesis; zebrafish; ER stress; actin cytoskeleton; mitochondria; glycolysis; TCA cycle

1. Introduction

Hyperhomocysteinemia (HHcy) is a metabolic abnormality characterized by unusually high plasma levels of Hcy, a sulfur-containing non-proteinogenic amino acid produced during the conversion of dietary methionine to cysteine. This pathological condition can arise either due to a nutritional deficiency of folate and B vitamins, required as cofactors in this pathway, or from a genetic abnormality in Hcy metabolism [1]. Both clinical and experimental studies in the last few decades strongly point out that HHcy is an independent risk factor for several pathologies like cardiovascular diseases, neurological and neuropsychiatric disorders, endothelial dysfunction and kidney diseases [2–4]. It is also reported that patients with severe HHcy frequently manifest cardiovascular complications that lead to their mortality [5,6]. In this line, the majority of the experimental studies have indicated cytotoxic damage of vascular endothelium in severe HHcy. Several previous studies have shown that high levels of Hcy can cause endothelial dysfunction through induction of apoptosis in Human Umbilical Vein Endothelial Cells (HUVEC) [7,8]. Increased level of oxidative stress is mostly reported as the main cause of this cellular toxicity and mitochondrial damage and dysfunction as a source of Reactive Oxygen Species (ROS) generation and consequent oxidative damage is the most accepted model in this context [9,10]. However, there are some opposing reports on HHcy-

 doi:10.20944/preprints202309.0215.v1

induced higher ROS generation [11] and HUVEC cell viability upon Hcy treatment [12]. Nevertheless, how HHcy induces mitochondrial dysfunction in endothelial cells is not fully understood. ER stress is yet another mechanism that has been repeatedly linked to severe HHcy associated vascular abnormalities, mostly in context of its role in inducing apoptotic cell death [13,14] and inflammation [15,16], but there is very little knowledge regarding the other functional consequences of ER stress in endothelial cells. In general, at population level, moderate HHcy is frequently observed due to aging and nutritional deficiency and a large number of epidemiological and clinical studies have provided compelling evidence that mild to moderate HHcy is associated with increased risk of developing several common vascular diseases including atherosclerosis, stroke and thrombosis [2,17,18]. However, there are lack of studies on how moderate HHcy affects endothelial function where unlike severe HHcy, no apparent cell death is observed.

One of the most important characteristic functional features of endothelial cells is angiogenesis and this process is primarily controlled by the canonical VEGF/VEGFR signaling [19]. At cellular level, the angiogenic process relies on two key cellular features, endothelial migration and proliferation. Previous reports have shown that severe HHcy inhibits angiogenesis, both *in vitro* and *in vivo* [20,21]. Moreover, impairment of endothelial migration and proliferation has also been reported during HHcy [22–24]. Though, compared to the consistent observation of HHcy induced migration defect, a study by Saha et al. reported that endothelial proliferation is not perturbed significantly upon Hcy treatment [25]. Regardless of this controversy, the exact mechanism by which HHcy causes endothelial migration and proliferation defect is still not clear. There are also disagreements regarding the association of canonical VEGF/VEGFR signaling, a key regulator of endothelial migration and proliferation, with HHcy. While some studies indicated it is reduced [26,27], others suggested it is increased [28,29] during HHcy. Additionally, how endothelial functional impairment like migration and proliferation defects are related to cytotoxicity, particularly in presence of moderate HHcy, remains largely unknown. Another peculiarity of the endothelial cells is their metabolic dependence on glycolysis. Even being highly glycolytic, in response to stress, endothelial cells can undergo metabolic maladaptation, which may act as a major contributing factor to vascular diseases [30,31]. In fact, widely established cardiovascular risk factors like hypercholesterolemia and diabetes are known to cause endothelial dysfunction through metabolic reprogramming [32]. Despite being a metabolic disorder, how HHcy influences metabolism of endothelial cells are less studied. In support of this possibility, a recent study revealed that HHcy accelerates metabolic reprogramming of activated B cells through the glycolytic protein PKM2 [33]. Recently, endothelial metabolism has also gained special attention in respect to the endothelial proliferation [34,35] and that indicates the need for further studies on metabolic changes in Hyperhomocysteinemic endothelial cells.

As the mechanism of endothelial dysfunction in HHcy is unclear, and the prevalence of mild to moderate HHcy is more frequent in population than the rare clinical condition of severe HHcy [36], here we studied the effect of sub-lethal HHcy on the functioning of endothelial cells. Using Hyperhomocysteinemic primary and immortalized HUVEC along with an *in vivo* zebrafish model we show that a moderate elevation of Hcy induces endothelial dysfunction independent of VEGF/VEGFR suppression and oxidative stress. We demonstrate that two independent axes control Hcy-induced endothelial migration and proliferation. Moderate HHcy causes endothelial migration defect by activating ER-stress associated adaptive UPR that leads to abnormal actin cytoskeleton remodeling and ER-stress blockers can rescue that migratory defect. However, sub-lethal HHcy induces impairment of endothelial proliferation through defective mitochondrial respiration and ATP production, independent of the ER-stress. Through metabolomics and metabolic flux analysis, we show an increase in both TCA cycle and glycolysis in moderate HHcy. We also demonstrate that Hcy-induced mitochondrial respiration-linked ATP loss was a result of dysfunctional ETC in endothelial cells. Reanalyzing an existent microarray data of moderate HHcy, we finally show that the mechanistic features of endothelial dysfunction in HUVECs are also conserved in adult Hyperhomocysteinemic endothelium which further strengthen our experimental results.

2. Materials and Methods

 doi:10.20944/preprints202309.0215.v1

2.1. Cell culture and chemical treatments

Immortalized human umbilical vein endothelial cell line (HUVEC/TERT2) was purchased from ATCC (CRL4053) and cultured in vascular cell basal medium (ATCC PCS100030) which was supplemented with endothelial cell growth kit-BBE (ATCC PCS100040). Primary human umbilical vein endothelial cell (HUVEC) was purchased from Thermo Fisher Scientific (C0035C) and grown in M200 medium (Thermo Fisher Scientific M200500) containing large vessel endothelial supplement (LVES) (Thermo Fisher Scientific A1460801). For transduction, Lenti-X HEK 293T cells (Clontech 632180) were cultured using DMEM high glucose medium (Gibco) which was supplemented with 10% FBS and 1X Antibiotic-Antimycotic. All the cells were maintained in a humidified incubation chamber with 5% CO_2 at 37°C. Cells were treated with freshly prepared and filter sterilized Hcy (Sigma-Aldrich H4628), Cys (Sigma-Aldrich C9768), 4-PBA (Sigma-Aldrich P21005) & TUDCA (Selleck Chemicals S3654) at indicated doses. For rescue experiments, 4-PBA and TUDCA pretreatments were done for 2 hours and 14 hours, respectively.

2.2. Zebrafish maintenance and morpholino microinjection

For all the *in vivo* experiments, adult wild type zebrafish (*Danio rerio*) line ASWT were used, unless otherwise stated. The double transgenic zebrafish line Tg(fli1a:EGFP; gata1a:dsRed) was a kind gift from Dr. Sridhar Sivasubbu's lab [37]. All the animals were bred, raised and maintained at 28.5°C on a 14 hour light/10 hour dark cycle and were housed in CSIR - Institute of Genomics & Integrative Biology (IGIB), New Delhi, India. All the experiments were done in compliance with the guidelines laid down by the Institutional Animal Ethics Committee. Care was taken to inflict minimal distress to the animals. Anti-sense morpholino oligonucleotides (MO) were designed and procured from Gene Tools (Philomath, OR, USA). Cocktail of translation blocking oligos against the two CBS isoforms of zebrafish - CBSa and CBSb were used along with a 5-base mismatch specificity control (SC MO). For knockdown of CTH also, a translation blocking morpholino (CTH MO) was used in addition to a 5-base mismatch specificity control (SC MO). Microinjection of MOs were done following our previously published protocol [38]. Injection replicates with at least 50 percent survival at 24 hpf (hours post fertilization) were considered for experiments. The sequences of the MOs used are as follows:

CBSa MO : 5'-GGGACTGAAGGCATTATTCCTCAAT-3'
CBSb MO : 5'-CTGGCATGGTTTACCCTGACTATCA-3'
CBS SC MO : 5'-GGCACTCAAGGCAATATACGTCAAT-3'
CTH MO : 5'-CTGCATCTCTGAAGACATGAGTGC-3'
CTH SC MO : 5'-TATGCATATCTGAACACATCAGTCC-3'

2.3. Lysate preparation

For lysis of cell samples, RIPA buffer supplemented with protease inhibitor cocktail (50X) and PhosStop (phosphatase inhibitor; 10X) was used. Lysis of the cells was done by incubating at 4°C in the lysis buffer for 30 minutes with slow rotation. Following incubation, the crude lysate was centrifuged at 10,000 rpm for 20 minutes at 4°C. After centrifugation, the supernatant was used as lysate. For zebrafish samples, an equal number of embryos were taken and then subjected to the same above-mentioned protocol except that embryos were homogenized in the NP-40 lysis buffer for about 10-20 seconds at 800 rpm followed by incubation for 30 minutes at 4°C.

2.4. Western blotting

Each sample was mixed with 2X Laemmli buffer and boiled at 95°C for 5 minutes. Equal amounts of protein (25-30 µg) for each sample were then loaded on the SDS-PAGE gel of appropriate percentage (10%-15%). After resolving, proteins were transferred from gel on PVDF membrane (0.2 µm) using wet transfer method at 4°C. Membranes were then blocked in 5% skimmed milk or 5% BSA (in case of IRE1p) either for 2 hours at room temperature (RT) or overnight at 4°C. Following blocking, membranes were incubated with the following primary antibodies overnight: anti-CBS

 doi:10.20944/preprints202309.0215.v1

(Abcam ab96252), anti-CGL (St. John's Laboratory STJ27874), Anti-GRP78 (BD 610979), Anti-IRE1p (Novus NB1002323), Anti-ATF4 (CST 11815), Anti-CHOP (CST 2895) and Anti-Actin (BD 612657). Membranes were washed three times in 1X TBST (0.1% Tween) for 15 minutes. Post washing, HRP-conjugated anti-rabbit or anti-mouse secondary antibodies (Amersham/GE) were added to the membranes and incubated for 2 hours. After that, membranes were again washed thrice with 1X TBST (0.1% Tween) for 15 minutes. Blots were developed by ECL chemiluminescent western blotting substrate using luminol and peroxide and the signals were captured in Syngene™ gel doc system (G:Box). Analysis of the protein bands to quantify fold change was done using ImageJ software.

2.5. RNA extraction and qPCR

For cells, RNA was extracted directly using the RNeasy mini kit as per manufacturer's protocol. For zebrafish, an equal number of embryos (25-30) were firstly homogenized in 1 ml Trizol™. After homogenization, 200 µl of chloroform was added to the samples followed by centrifugation at 10,000 rpm for 15 minutes and carefully only the aqueous phase is taken for the next step. The aqueous phase was mixed with 500 µl of absolute ethanol and applied to the columns provided in the RNeasy mini kit (Qiagen). Thereafter, all the subsequent steps were followed as per manufacturer's instructions in the kit. Equal amount of RNA (1 µg) was used to prepare the cDNA using Verso™ cDNA synthesis kit. qPCR run was carried out on a LightCycler 480 system (Roche). All experiments were performed in a 384-well plate with triplicates of each sample. The details of the primers used are given in Table S1. Results were normalized with 18S.

2.6. Homocysteine measurement

Intracellular Hcy concentration was measured by HPLC. Samples were lysed using RIPA buffer. After that, 100 µl of the lysate was taken and then treated with 35 µl of 1.43 M sodium borohydride in 0.1 M NaOH (for reduction of disulfide bonds). Next, in order to avoid foaming, 10 µl of amyl alcohol was added. Thereafter, addition of 35 µl of 1 M HCl was done. To this mixture, 50 µl of 7 mM Bromobimane in 5 mM sodium EDTA (pH 7.0) was added (for conjugation of the reduced thiols with fluorophore) and the solution was then incubated at 42°C for around 15 minutes followed by incubation at RT for another 30- 45 minutes. For precipitation of intracellular proteins, 50 µl of 1.5 M perchloric acid was used followed by centrifugation at 12000 rpm for 10 minutes. Then, neutralization of the supernatant was done with 6 µl of 2 M Tris base. For injection, 4 µl of derivatized sample was then used and this was loaded into a 100×4.6 mm,1.8 micron Eclipse plus C18 column using Agilent-1260 Ultra-high performance liquid chromatography (UPLC). Equilibration of the Column was done with 90% buffer A (composed of 5% methanol and 0.86% acetic acid in water) and 10% Buffer B (100% methanol). Lastly, elution of thiols were done by linear gradient of both buffers (from 90% Buffer A, 10% Buffer B to 0% Buffer A and 100% buffer B in 7 minutes). A flow rate of 0.7 ml/min was maintained at RT. Estimation of Hcy level was done by measuring the area for the homocysteine-bimane peak followed by calculation of its concentration using a regression equation derived from a standard curve.

2.7. Trypan blue exclusion assay

Endothelial cells at a density of $8x10^4$ were seeded to each well of a 12-well flat bottom culture plate. Following treatment, live as well as dead cells (floaters) were collected and then centrifugation was done at 3000 rpm for 5 minutes. After that, the supernatant was discarded and cells were dissolved in 1X PBS. For staining, 10 µl of the cell suspension was mixed with 0.4% trypan blue solution (Gibco) and then incubated for 2 mins at RT. Live cells (trypan negative) and dead cells (trypan positive) were counted with the help of a hemocytometer and cell death was represented in percentage of dead cells.

2.8. Tube formation assay

 doi:10.20944/preprints202309.0215.v1

Control and 2 mM Hcy treated (24 hours) HUVEC/TERT2 cells were used for the tube formation assay. Firstly, wells of a 48-well plate were coated with 125 µl of Matrigel™ (Corning 356234) matrix by adding the Matrigel™ towards the center of the well and then spreading with a tip. During coating, Matrigel™ was kept on ice and pre-chilled 48-plate and tips were used. While adding Matrigel™ to the wells, special care was taken to avoid creating any bubbles by not squeezing the pipette till the very last stop. The plates were then kept at 37°C for 1 hour. After coating, 150 µl of untreated or Hcy treated cell suspension (40,000 cells/well) in complete growth medium was added to each well. Lastly, the plates were incubated at 37°C for 3-4 hours followed by bright field imaging at 4X magnification. Measurement of total tube length and number of branches were done for three different fields in each well using the Angiogenesis Analyzer plugin in ImageJ [39].

2.9. Scratch wound assay

Cells were plated in a 12-well plate ($1x10^5$) and cultured till 100% confluency. After that, cells were starved in incomplete growth medium (without serum and growth factors) for 8 hours. Following starvation, manually two straight line scratches were created diametrically perpendicular to each other through the center of the plate with a P200 pipette tip and the cells were allowed to migrate for 24 hours in presence of Hcy and/or other chemicals (Cys, 4-PBA, TUDCA). To exclude cellular proliferation induced changes, Mitomycin C (Sigma-Aldrich) was added to each well at a final concentration of 1 µg/ml. Just before imaging, scratches for 0 hour time points were made in separate wells of the same plate. Cells were then fixed by adding a fixing solution (37% formaldehyde and 0.2% Glutaraldehyde in PBS) followed by 10 minutes of incubation at RT and finally bright field images were obtained at 10X magnification. Migrated cells were counted from 6 different image fields from each well using ImageJ software and the difference was reported as fold change in migrated cells.

2.10. BrdU incorporation assay

Proliferation of cultured human endothelial cells was estimated by BrdU Cell Proliferation ELISA kit (Roche), following manufacturer's protocol. Briefly, $1x10^4$ cells were seeded in a 96-well flat bottom plate containing 100 µl media in each well. After that, BrdU labeling solution was added to the cells (final concentration: 10 µM. Per well). The plate was then incubated for 3 hours in a cell culture incubator at 37°C. The BrdU containing media was then removed and cells were fixed and denatured by adding FixDenat for 30 minutes at RT. After removing FixDenat, cells were incubated with 100 µl of anti-BrdU-peroxidase (POD) working solution for 90 minutes at RT. Antibody conjugate was then removed and the cells were washed thrice with 200 µl of 1X PBS. Finally, to each well, 100 µl of substrate solution was added and after 2-5 minutes the absorbance was measured in a microplate reader at 370 nm taking 492 nm as reference wavelength.

2.11. Measurement of mitochondrial membrane potential

Mitochondrial membrane potential was quantified using a potentiometric dye called Tetramethylrhodamine ethyl ester or TMRE (Invitrogen). Cells were seeded at $1x10^4$ density in a black 96-well plate with flat clear bottom. After Hcy treatment, TMRE was added to each well at a final concentration of 400 nM and then the plate was incubated for 10 minutes in the dark at 37°C. As a positive control, prior to TMRE addition, cells were incubated with an uncoupler called carbonyl cyanide m-chlorophenyl hydrazone or CCCP (Invitrogen) at final concentration of 500 µM for 10 minutes at 37°C in the dark. Fluorescent intensities were measured in a microplate reader with 549 nm and 575 nm as excitation and emission wavelengths, respectively.

2.12. Measurement of cellular reactive oxygen species (ROS)

Total cellular ROS in HUVEC/TERT2 cells was analyzed using the fluorescent dye 2′, 7′-dichlorodihydrofluorescein diacetate (CM-H2DCFDA, Invitrogen). Briefly, $1x10^4$ cells were seeded in a black 96-well plate with flat clear bottom. Next day, cells were treated with Hcy for 24 hours. Post

 doi:10.20944/preprints202309.0215.v1

Hcy treatment, CM-H2DCFDA was added to each well at a final concentration of 25 μM followed by incubation at 37°C for 15 minutes in the dark. Before CM-H2DCFDA addition, positive control wells were subjected to 1 mM H_2O_2 treatment for 10 minutes. Mean fluorescent intensities were measured using a microplate reader taking 492 nm as excitation wavelength and 517 nm as emission wavelength.

For zebrafish embryos, 2 dpf embryos were exposed to 5 μM CM-H2DCFDA in embryo water and incubated for 20 minutes at 28.5°C. After that, embryos were washed three times with embryo water. Finally general ROS was observed under the green channel of Axioscope A1 (Zeiss) fluorescence microscope. For positive control, 1 mM H_2O_2 was used.

2.13. Generation of mitoGFP transduced cells

For lentivirus transduction, pLYS1-FLAG-MitoGFP-HA (Addgene 50057) plasmid was used. Transfection of the cells and collection of lentiviral particles were performed as per our previously published protocol [40].

2.14. Confocal imaging of mitoGFP transduced cells

To check mitochondrial morphology, MitoGFP transduced cells were grown on coverslips in a 6-well plate. Post Hcy treatment, cells were fixed using the aforementioned fixing solution for 10 minutes at RT. After a wash with 1x PBS, cells were mounted on the slides using ProLong Gold mounting solution with DAPI (Invitrogen). Images were captured by Nikon confocal A1R HD attached with Ti2-E (Nikon, Japan) using 60X Nikon objective (1.42 NA).

2.15. Mitochondrial length measurement

Measurement of mitochondrial size in MitoGFP transduced HUVEC/TERT2 cells was done using ImageJ as per our previously published protocol [41]. Briefly, three channels from the images were separated and then the green channel was selected for (labeled mitochondria) sharpening. After that, despeckle, background subtraction and enhancement of local contrast were done. Considering mitochondria as a filamentous tube-like structure, a filter called 'tubeness' (sigma = 0.0210) was imposed to increase the filamentous feature of segmented mitochondria. After that, gaussian blur (sigma radius = 1.000) was applied before finally converting the image to binary. This image was then used to measure mitochondrial length.

2.16. Rhodamine phalloidin staining

F-actin staining of endothelial cells was done using rhodamine labeled phalloidin. At first, HUVEC/TERT2 cells were grown on coverslips in a 6-well plate. After treatment, cells were fixed using previously mentioned fixing solutions for 10 minutes at RT. Then, one wash with 1X PBS was given. Thereafter, cells were permeabilized in 0.1% Triton X-100 in PBS for 5 minutes at RT to increase permeability. Samples were then washed twice in 1X PBS. Stock solution (400x in DMSO) of rhodamine phalloidin (Invitrogen) was diluted (2.5 μl in 1 ml of PBS) and then added to the samples followed by incubation in a cell culture incubator at 37°C for 60 minutes. Then the samples were washed three times with 1X PBS. Finally, coverslips were mounted using Prolong Gold mounting solution with DAPI. Confocal images were acquired using Nikon confocal A1R HD attached with Ti2-E. Images were captured using a 100x Nikon objective (1.45 NA).

2.17. Zebrafish imaging and heartbeat measurement

For imaging, MO injected embryos were immobilized in 2.5% methyl cellulose and bright field images were taken at 48 hpf using Nikon SMZ800N Stereomicroscope at 5X magnification. Fluorescent images were captured in Zeiss Axioscope A1 (Carl Zeiss, Germany) at 5X magnification under GFP channels. To study intersegmental vessels, zebrafish embryos were mounted in low melting point agarose and confocal imaging was performed using Leica SP8 TCS microscope (Leica, Germany) at 10X magnification. Images were captured and processed with Zeiss AxioVision 4.6 and

 doi:10.20944/preprints202309.0215.v1

Leica LAS X softwares, respectively. Heartbeat of the embryos was measured by the stopwatch count method. Analysis of zebrafish vasculature and pericardial area was done using the ImageJ software.

2.18. Glucose uptake assay

After 24 h of Hcy treatment, cells were replenished with HBSS containing 2-NBDG (Invitrogen) of 10 μM final concentration and incubated at 37°C for 30 minutes. Fluorescence was measured in a microplate reader with 475 nm and 550 nm as excitation and emission wavelengths respectively.

2.19. Extracellular flux analysis

Oxygen consumption rate (OCR) and extracellular acidification rate (ECAR) was measured using Seahorse XF24 extracellular flux analyzer (Agilent Technologies). HUVEC/TERT2 cells were seeded at a density of $8x10^4$ per well. As per manufacturer's protocol, Mitochondrial stress test was performed in basal condition as well as in stressed condition in presence of 1 μM oligomycin, 1 μM FCCP and 0.5 μM rotenone/antimycin A (all from Agilent). Glycolysis stress test was run in basal condition and in presence of 10 mM glucose, 1 μM oligomycin and 25 mM 2-deoxy-glucose or 2-DG (all from Agilent). OCR and ECAR values quantified by these experiments were normalized to total protein content of each sample, calculated by performing BCA assay after each run. For analysis, pre-standardized tools in the Seahorse Wave software were used.

2.20. Metabolite extraction and targeted metabolomics

Treated and non-treated HUVEC/TERT2 cells were harvested, washed once with ice-cold PBS followed by centrifugation for 5 minutes at 1500 rpm (in 4°C). Then, cells were resuspended in pre-chilled methanol : water (80% : 20 % respectively) solution for approximately 10 minutes with intermittent vortexing. This suspension was then centrifuged at 10,000 rpm for 15 minutes in 4°C. Thereafter, the supernatant was collected and transferred into a fresh microcentrifuge tube and vacuum dried in a vacuum concentrator in alcoholic mode at 30°C. The lyophilized metabolite was then re-suspended in 0.1% formic acid in water, vortexed and centrifuged at 10,000 rpm for 5 minutes. Sufficient volume of supernatant was then transferred into micro volume inserts and injected into the LC/MS system.

Data acquisition was done using a Thermo TSQ - Altis triple stage quadrupole mass spectrophotometer in dual polarity (both positive and negative) mode. The instrument voltage was as follows : capillary voltage = 3500V and 3000V for positive and negative mode respectively. Onto a UPLC BEH HILIC column (Waters Corp.), 10 μl of sample was loaded. Metabolites were eluted from the column at a flow rate of 0.300 ml/min. The mobile phase consisted of a linear gradient of 100% LC grade water with 0.1% formic acid (Buffer A) and 95% Acetonitrile with 0.1% formic acid (Buffer B). Relative quantification was performed using Skyline software (version 1.2.2). The optimized parameters of all the different measured metabolites are given in Table S2. Fold change in peak area was calculated and represented as fold change in AUC (area under curve).

2.21. Analysis of available microarray dataset

The microarray dataset GSE175735 from Gene Expression Omnibus (GEO) database was used to understand the effect of HHcy on human adult endothelial cell line (HAEC) [42]. Files were extracted and imported into R using the *readAffy()* function. Samples were pre-processed in order to remove any systematic error such as background noise and dye bias. Pre-processing involves quantile normalization and background correction using *rma()* function. Then gene probes were annotated with respective Gene IDs by *hugene10sttranscriptcluster.db* package. Thereafter differentially expressed genes (DEGs) between Hcy treated (three replicates) and control samples (three replicates) were obtained using the *limma* package. Genes with p-value < 0.05 were considered for DEG analysis. After that, DEGs were mapped to KEGG (Kyoto Encyclopedia of Genes and Genomes) pathways. For this purpose, all the gene entries from Cell Cycle (has04110), Migration (hsa04670), UPR (has04141), Glycolysis (hsa00010), TCA cycle (hsa00020), Angiogenesis (has04370) and Antioxidants (hsa05208)

 doi:10.20944/preprints202309.0215.v1

were downloaded. Heatmaps of DEGs were plotted for each pathway using the *coolmap()* function of the *limma* package [43].

2.22. Statistical analysis

All the data are from three independent experiments. Quantitative statistical data are reported as means ± SEM. Calculation of statistical significance was done by unpaired Student's t-test and represented by asterisk with *P≤0.05, **P≤0.01, ***P≤0.001, ****P≤0.0001 and ns as non-significant (P>0.05). All the graphs were made using GraphPad Prism (GraphPad Software, La Jolla, USA).

3. Results

3.1. Moderate increase in Hcy levels causes endothelial dysfunction

In order to understand the effect of moderate HHcy on endothelial function, we first exposed immortalized human endothelial cell line HUVEC/TERT2 to various doses of Hcy for 24 hours. Cell death analysis by Trypan blue exclusion assay showed that Hcy can cause cytotoxicity in endothelial cells in a dose dependent manner. Although, we found that even at a very high concentration, the amount of cell death was below 15% which indicates a moderate impact of Hcy on survival of endothelial cells (Figure 1A). To further negate the effect of cytotoxicity on subtle endothelial function, we chose 2 mM concentration (24 hours) for all our subsequent experiments as at this dose no statistically significant cell death was observed. Measurement by HPLC revealed that at 2mM treatment concentration, intracellular Hcy levels was increased by four fold that confirmed a moderate Hyperhomocysteinemic condition (Figure 1B). To study the functional consequence of sub-lethal HHcy on endothelial cells, we performed tube formation assay. As shown in the representative images, tube formation was drastically hampered upon Hcy treatment (Figure 1C). Quantitative analysis also revealed that in comparison to untreated cells, total tube length and number of branches were reduced by around 50% in Hcy treated cells (Figure 1D and 1E). Overall, we found that sub-lethal Hcy exposure leading to induction of moderate HHcy can detrimentally influence endothelial function.

Preprints (www.preprints.org) | NOT PEER-REVIEWED | Posted: 5 September 2023 doi:10.20944/preprints202309.0215.v1

Figure 1

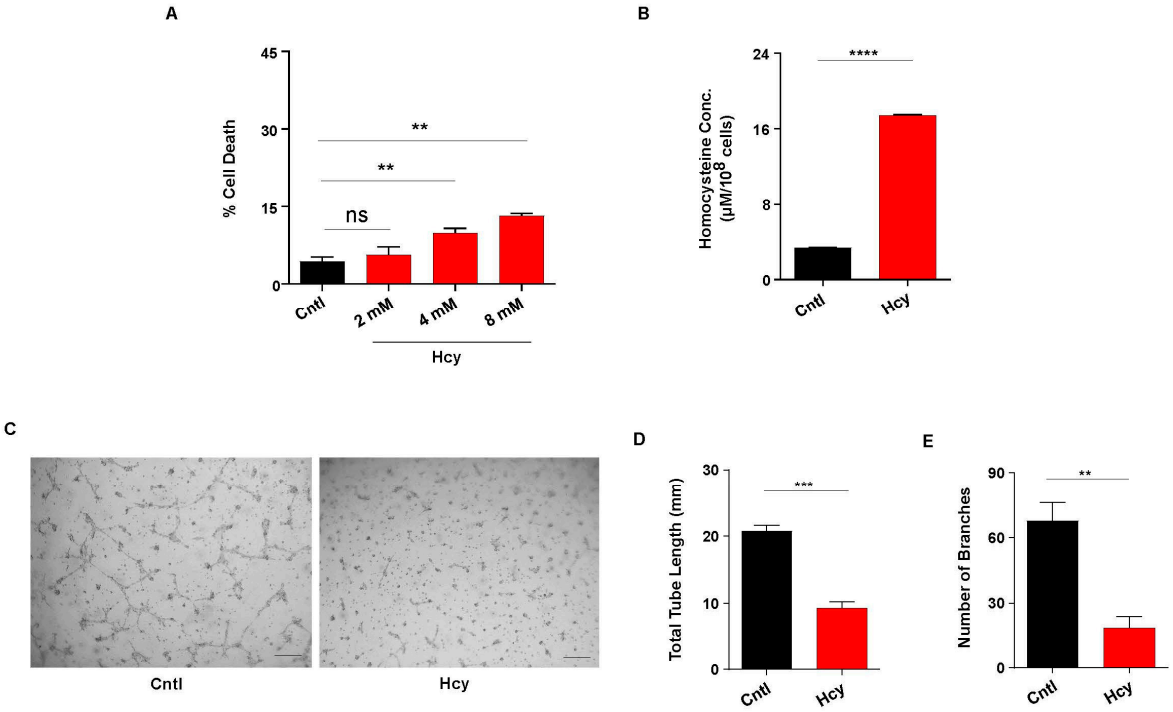

Figure 1. Sub-lethally increased Hcy causes endothelial dysfunction. (A) Bar graph represents percentage of cell death in HUVEC/TERT2 cells treated with increasing concentration of Hcy. A non-cytotoxic concentration of 2 mM was chosen for all the subsequent experiments. (B) HPLC mediated quantification of intracellular Hcy concentration in HUVEC/TERT2 cells revealing induction of moderate Hyperhomocysteinemic condition post 2 mM Hcy treatment for 24 h. (C) Representative images of tube formation assay showing functional abnormality in Hcy treated HUVEC/TERT2 cells as compared to untreated cells. Scale bar, 250 µm. (D) & (E) Respective quantifications showing total tube length and number of branches formed during tube formation assay are drastically reduced upon 2 mM Hcy treatment for 24 h. Data are shown as Mean±SEM with n ≥ 3. **P≤0.01, ***P≤0.001, ****P≤0.0001 and ns is non-significant (P>0.05).

3.2. Moderate HHcy impairs endothelial migration and proliferation without suppressing VEGF signaling and generating oxidative stress

Next, we wanted to investigate how a sub-lethal dose of Hcy affects migration and proliferation, two critical parameters of endothelial function. Scratch wound assay in presence of proliferation blocker Mitomycin C revealed that at a non-cytotoxic concentration, Hcy can significantly impair endothelial migration (Figure 2A and 2B). Moreover, BrdU incorporation assay showed that endothelial proliferation is also inhibited by around 20% upon Hcy treatment (Figure 2C).

To check whether the above-mentioned effects of sub-lethal HHcy are conserved in a more physiological cellular set-up of primary endothelial cells, we used primary HUVEC. We confirmed that the treatment of primary HUVEC with 2 mM concentration of Hcy for 24 hours faithfully recapitulated the defects in migration and proliferation at the absence of cellular toxicity, as observed in HUVEC/TERT2 cells (Figure S1A - C). These results demonstrated that the functional response of HUVEC/TERT2 towards exogenous Hcy was comparable to that of primary endothelial cells.

Then we tested whether the observed functional abnormalities were specific to Hcy and not a general response of endothelial cells toward any high sulfhydryl group containing metabolite. To verify this, we exposed HUVEC/TERT2 cells to 2 mM of Cysteine, another sulfhydryl group

Preprints (www.preprints.org) | NOT PEER-REVIEWED | Posted: 5 September 2023 doi:10.20944/preprints202309.0215.v1

containing amino acid from the same metabolic pathway, for 24 hours. Through scratch wound assay we observed that in contrast to Hcy, treatment with Cysteine did not alter migration of endothelial cells (Figure 2D and 2E). Similarly, BrdU incorporation assay showed that unlike Hcy, proliferation of endothelial cells also did not change significantly upon Cysteine exposure (Figure 2F). Since a number of previous studies have implicated canonical VEGF/VEGFR signaling, a master regulator of endothelial migration and proliferation, with HHcy-associated vascular dysfunction [26,28], we assessed the expression levels of VEGFA ligand and its cognate receptors VEGFR1 and VEGFR2. As shown by qPCR data, sub-lethal Hcy treatment did not cause suppression of VEGF/VEGFR signaling (Figure 2G). Another mechanistic aspect that has been most frequently linked with HHcy induced vascular endothelial dysfunction is oxidative stress [9,10]. Intriguingly, total ROS measurement using general ROS indicator CM-H2DCFDA showed that 2 mM Hcy treatment did not cause oxidative stress in endothelial cells (Figure 2H). As a whole, these data indicate that sub-lethal HHcy can specifically impede endothelial migration and proliferation, which is not related to inhibition of VEGF/VEGFR signaling and increased ROS production.

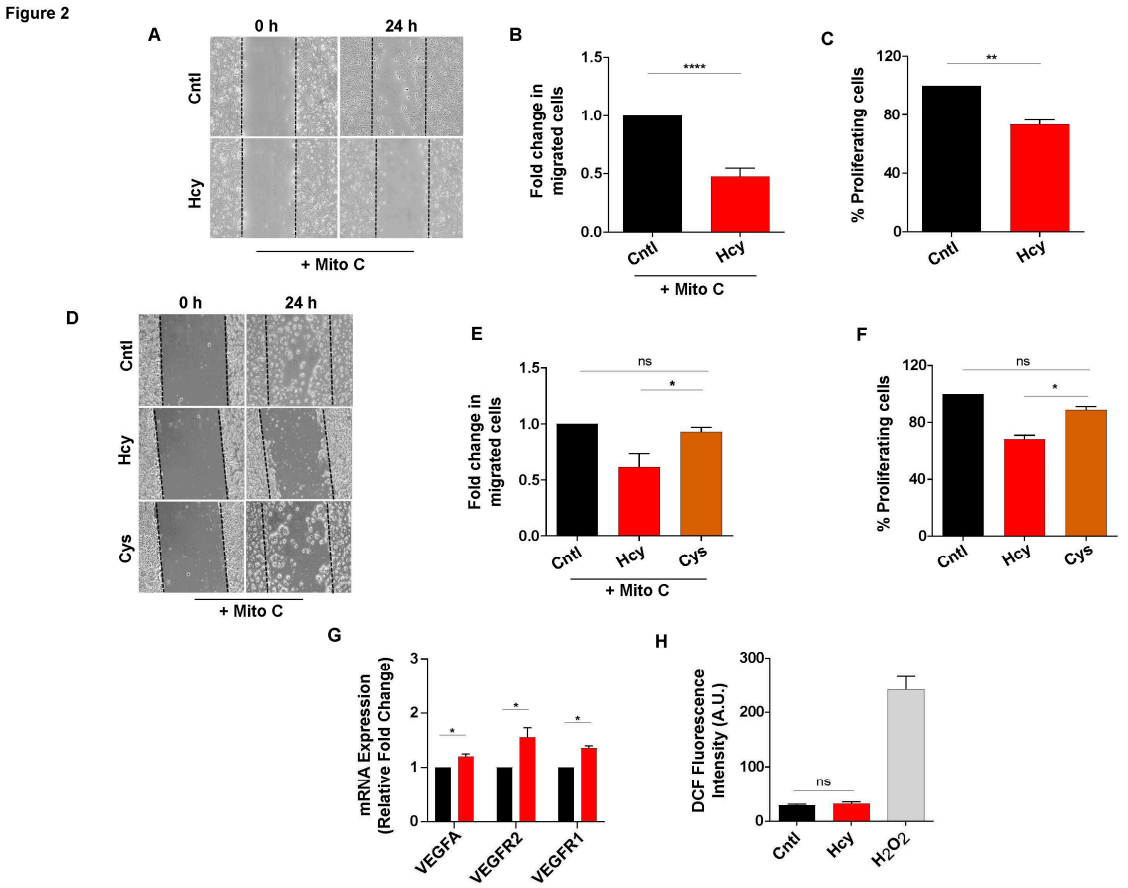

Figure 2. Sub-lethal HHcy reduces endothelial migration and proliferation without inhibiting VEGF signaling and generating oxidative stress. (A) Scratch wound assay in presence of Mitomycin C showing less migrated endothelial cells at 24 h post 2 mM Hcy treatment. (B) Quantification of migrated cells revealing that endothelial migration is significantly reduced in Hcy treated cells compared to control cells. (C) Bar plot of BrdU cell proliferation assay indicating that 2 mM Hcy treatment for 24 h causes proliferation defect in endothelial cells. (D) Representing scratch wound assay images depicting that as opposed to Hcy treatment, a similar concentration of Cys did not affect migration of endothelial cells when compared with untreated cells at 24 h. (E) Bar plot of measurement of migrated cells in scratch wound assay showing that contrary to Hcy treated cells, fold change in migrated cells is not altered upon 2 mM Cys treatment for 24 h as compared to control cells. (F) BrdU cell proliferation assay revealing that unlike Hcy treated cells, 2 mM Cys treatment for 24 h did not influence endothelial proliferation. (G) Bars showing that compared to untreated cells, exposure to sub-lethal Hcy caused upregulation of mRNA levels of canonical VEGF

 doi:10.20944/preprints202309.0215.v1

signaling markers. 18S was used as internal control. (H) Bar graph showing that sub-lethal Hcy treatment does not induce ROS production in endothelial cells as determined by the fluorescent probe CM-H2DCFDA. For positive control, H2O2 was used. Data are shown as Mean±SEM with n ≥ 3. *P≤0.05, **P≤0.01, ****P≤0.0001 and ns is non-significant (P>0.05).

3.3. Generation of in vivo knockdown models of CBS and CGL, transsulfuration pathway regulators involved in Hcy catabolism

To examine whether the observed functional implications of sub-lethal HHcy on vascular endothelial cells is conserved *in vivo*, we used zebrafish as a model organism. For this purpose, we targeted CBS, the rate limiting enzyme of the transsulfuration pathway that catalyzes the conversion of Hcy to cystathionine [44] (Figure 3A). As our goal was to study the effect of moderate HHcy, we used a genetic knockdown (KD) approach in our model generation instead of a CBS knockout (KO) model which mimic Homocystinuria, a severe form of HHcy [6,45]. To generate moderate HHcy in zebrafish, we used a cocktail of translation blocking morpholino oligonucleotides (MOs) targeting the ATG regions of two zebrafish paralogs CBSa and CBSb (referred to as CBS MO hereafter). We also incorporated a 5-base mismatched specificity control MO (SC MO) to generate control embryos. For translational knockdown, MOs were microinjected at 1 cell stage and then embryos were observed at 2 days post fertilization (dpf) as by this time most of the components of the cardiovascular system have already developed. At first, we confirmed the efficacy of the MOs through western blotting which revealed that CBS is significantly downregulated in CBS MO injected embryos (morphants) compared to SC MO injected embryos. We also checked the protein level of CGL, the downstream gene of CBS, as a negative control and found that CGL level is not altered in CBS MO injected embryos (Figure 3B). Moreover, HPLC mediated measurement from our lab previously established that knockdown of CBS in zebrafish embryos can cause 4-5 fold increase in Hcy levels representing moderate HHcy [46]. Next, we checked the viability of CBS MO and SC MO injected embryos and found that moderate HHcy is not lethal *in vivo* which nicely corroborates with our cellular model data (Figure 3C). Additionally, when compared to the anatomy of SC MO injected embryos, sub-lethal HHcy did not cause any apparent gross morphological defect in CBS MO injected embryos (Figure 3D).

Transsulfuration pathway acts as the major intracellular source of Cysteine and the first enzymatic step of this pathway is governed by CBS. Thus, we wondered whether general perturbation of the transsulfuration pathway would mimic the effect of HHcy on the vasculature *in vivo*. To check that, we also generated an *in vivo* zebrafish model of Cystathioninuria, a clinical condition associated with deficiency of CGL [47], the second enzyme of transsulfuration pathway [44] (Figure 3A). Similar to generation of Hyperhomocysteinemic embryos, a translation blocking MO against the ATG start site of CGL was used along with a 5-base mismatch specificity control. At first, western blotting of the embryo lysates confirmed that CGL is significantly downregulated in the morphant embryos. Although CBS, which is the upstream gene of the pathway, remained unaltered in the morphant embryos suggesting the morpholino is specific and functional (Figure 3E). As is the case with HHcy, viability of the morphant embryos did not decline significantly (Figure 3F) and there were no obvious gross morphological defects in CGL deficient embryos (Figure 3G). Thus, we have generated *in vivo* models to study the response of vasculature towards sub-lethal HHcy as well as a disturbed transsulfuration pathway *per se*.

Preprints (www.preprints.org) | NOT PEER-REVIEWED | Posted: 5 September 2023 doi:10.20944/preprints202309.0215.v1

Figure 3

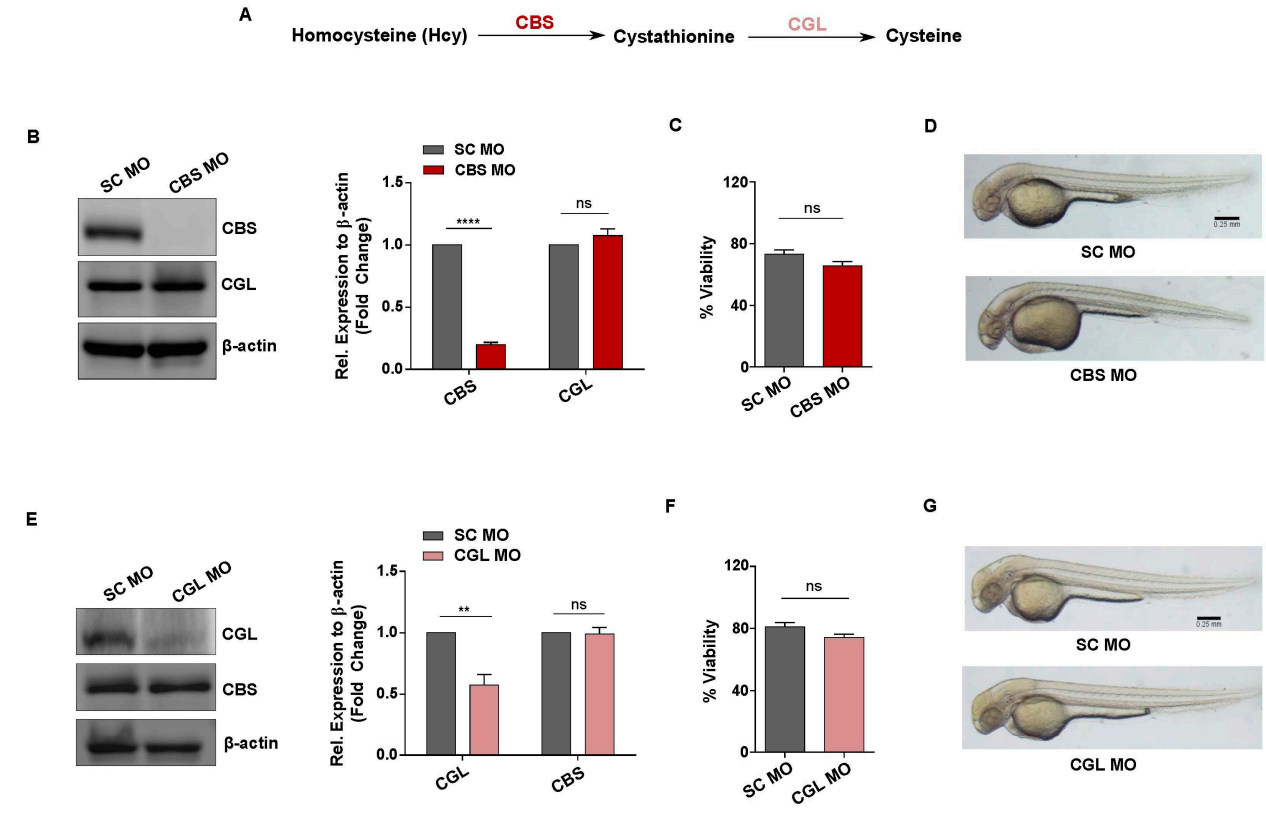

Figure 3. Generation of in vivo knockdown models of CBS and CGL, regulators of transsulfuration pathway involved in Hcy catabolism.(A) Simplified diagram showing the enzymes and metabolites of transsulfuration pathway (B) Representative western blot of 2 dpf embryos lysates showing that as compared to SC MO injected embryos, CBS protein level is downregulated in CBS MO injected embryos. Expression of CGL, the other enzyme of the same pathway, remained unaltered. As a loading control β-actin was used. Corresponding bar plot showing fold change in protein expression (normalized to β-actin) as determined by densitometric analysis of the protein band. (C) Bar plot revealing no statistically significant difference in the viability of scrambled control and Hyperhomocysteinemic CBS MO embryos. (D) Bright field images exhibiting no apparent gross morphological defect in CBS morphants as compared to scrambled Mo injected embryos of 2 dpf. Scale bar, 0.25 mm. (E) Representative western blot of embryo lysates at 2 dpf showing reduced protein level of CGL in the embryos injected with CGL MO. Expression of CBS, the upstream protein of the same pathway, remained unaltered. β-actin was used as a loading control. Corresponding bar diagram showing densitometric analysis of the fold change in protein expression (normalized to β-actin). (F) In comparison to SC MO injected embryos, viability of CGL MO injected embryos were not altered significantly. (G) Representative bright field images showing absence of any gross morphological defect in CGL MO injected embryos as compared to SC MO injected ones at 2 dpf. Scale bar, 0.25 mm. Data are shown as Mean±SEM with n ≥ 3. **P≤0.01, ****P≤0.0001 and ns is non-significant (P>0.05). .

3.4. Moderate HHcy induces vascular abnormality in vivo without inhibiting VEGF signaling and inducing oxidative stress

In order to assess vascular endothelial function upon induction of sub-lethal HHcy in zebrafish embryos, we used transgenic zebrafish line Tg(fli1a:EGFP;gata1a:DsRed) where endothelial cells express EGFP under the fli1a promoter and analyzed caudal vein plexus (CVP) and intersegmental vessel (ISV) formation, two angiogenic events of distinct anatomical regions occurring at different

Preprints (www.preprints.org) | NOT PEER-REVIEWED | Posted: 5 September 2023 doi:10.20944/preprints202309.0215.v1

time points [48]. Compared to the normal sprouting angiogenesis of SC MO injected embryos, we observed that formation of CVP sprouts are drastically reduced in CBS MO injected embryos (Figure 4A, left panel). Upon quantification we found a 50% decrease in the number of CVP sprouts of the morphant embryos (Figure 4B). Likewise, in comparison to SC MO injected embryos, the angiogenic sprouts associated with ISV formation appeared to be irregular, incomplete and abnormally branched in the morphant embryos (Figure 4A, right panel). Percentage of embryos with normally formed ISV also found to be severely reduced in CBS MO injected embryos (Figure 4C). Furthermore, phenotypic screening revealed that around 80% of embryos with sub-lethal HHcy exhibited angiogenic abnormalities (Figure 4D). Interestingly, apart from vascular dysfunction, the morphant embryos later (4 dpf) developed severe pericardial edema characterized by a tubular heart (Figure S2A) and significant increase of the pericardial area (Figure S2B). Along with cardiac structural anomaly, we also observed functional impairment in terms of reduction of heart beat of morphant embryos as compared to SC MO injected ones (Figure S2C). As opposed to Hyperhomocysteinemic embryos, CGL deficient embryos showed no evident anatomical differences in the vasculature when compared to control embryos (Figure 4E). Percentage of embryos with angiogenic abnormalities were also not significantly higher in CGL morphants (Figure 4F). Therefore, we found that perturbation of the transsulfuration pathway cannot by itself cause vascular dysfunction *in vivo*. Nevertheless, similar to our cellular model, we also checked the status of canonical VEGF signaling markers in the embryos with sub-lethal HHcy and found that mRNA levels of VEGFAA, VEGFR2 and VEGFR1 are not reduced (Figure 4G). Furthermore, general ROS indicator CM-H2DCFDA mediated staining revealed that although there is a sharp increase in oxidative stress levels of the pericardial region, CVP and ISV forming regions of hyperhomocysteinemic embryos have no such striking changes. In contrast, H_2O_2 treated positive control embryos have increased ROS production not only in the pericardial region but also in the tail and trunk, CVP and ISV forming anatomical parts respectively (Figure 4H). As a whole, these results suggest that sub-lethal HHcy can specifically cause vascular endothelial dysfunction *in vivo* and as is the case with our cellular model data, it is not associated with inhibition of VEGF/VEGFR signaling and oxidative stress induction.

Figure 4

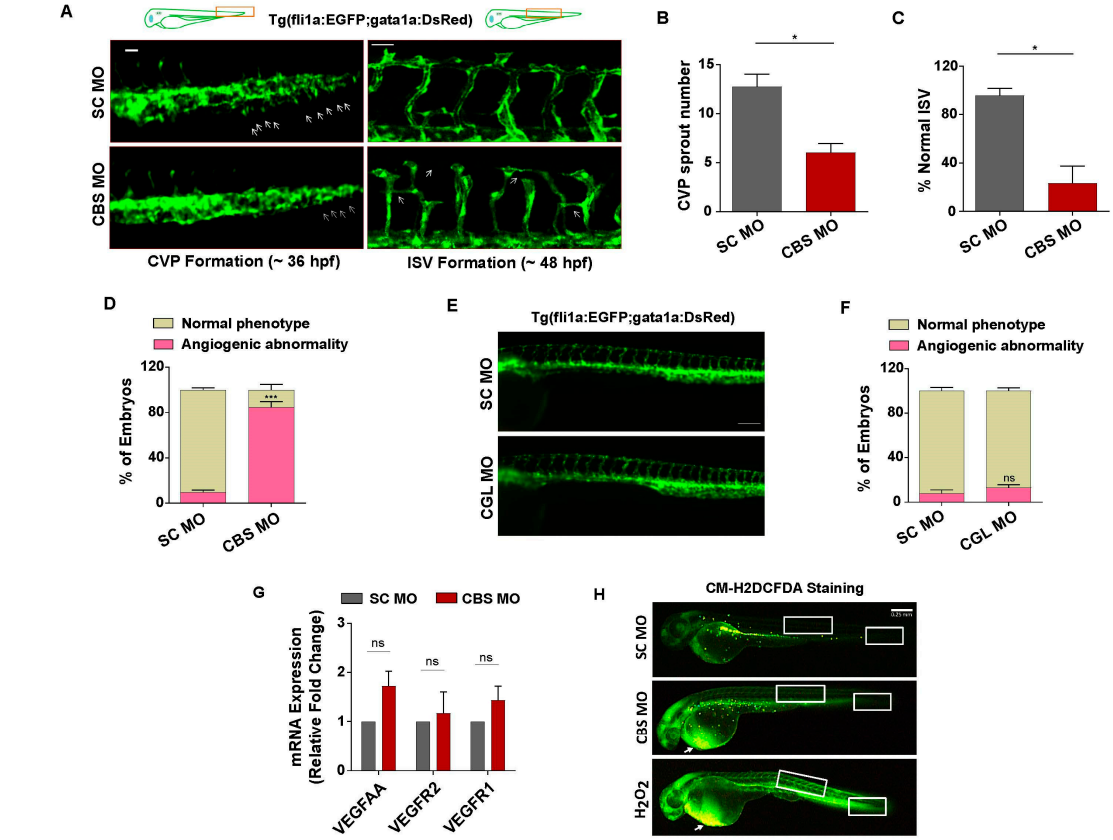

 doi:10.20944/preprints202309.0215.v1

Figure 4. Sub-lethal HHcy causes vascular abnormality in vivo without inhibiting VEGF signaling and inducing oxidative stress. (A) Upper panel: schematic illustration of transgenic zebrafish line Tg(fli1a:EGFP;gata1a:DsRed) showing anatomical position (rectangle) of CVP and ISV forming area in 36 hpf and 48 hpf embryos respectively. Left panel: representative images revealing impairment in sprouting angiogenesis during CVP formation of CBS morphants. Arrows are depicting CVP sprouts. Scale bar, 0.05 mm. Right panel: representative confocal images showing abnormal ISV formation in CBS morphants compared to SC MO injected embryos. Arrows indicating incomplete, irregular and abnormally branched ISVs. Scale bar, 50 μm. (B) & (C) Bar plots respectively showing CVP sprout number and percentage of normal ISV are significantly reduced in CBS morphants. (D) Bar diagram depicting percentage of embryos with angiogenic abnormality is significantly higher in CBS MO injected embryos compared to SC MO injected ones. (E) Representative fluorescent images showing no observable difference in the vascular anatomy of SC MO and CGL MO injected embryos at 2 dpf. Scale bar, 0.2 mm. (F) Bar plot depicting no significant change in percentage of embryos with observable angiogenic abnormality in CGL morphants compared to SC MO injected ones. (G) Bars showing mRNA expression levels of canonical VEGF signaling markers in CBS MO and SC MO injected embryos at 2 dpf. 18S was used as internal control. (H) Representative images depicting location of oxidative stress in 2 dpf zebrafish embryos, detected using general ROS indicator CM-H2DCFDA. White arrows showing drastic increase of ROS levels in the pericardial area of CBS morphants and H2O2 treated embryos. White boxes of the tail and regions representing sites of previously observed CVP and ISV angiogenesis, respectively. Scale bar, 0.25 mm. Data are shown as Mean±SEM with $n \geq 3$. *P≤0.05, ***P≤0.001 and ns is non-significant (P>0.05). .

3.5. Adaptive UPR activation controls endothelial migration defect in moderate HHcy

Since we have found that sub-lethal HHcy invokes a similar functional abnormality *in vitro* and *in vivo*, which is independent of VEGF/VEGFR suppression and oxidative stress induction, we next focused to elucidate the mechanism by which migration and proliferation is impaired in Hyperhomocysteinemic endothelial cells. In the context of Hcy induced cytotoxicity, generation of ER stress is a common mechanism that has been frequently linked in both endothelial [13,49,50] and other cell types [51,52]. As a response to ER stress, the unfolded protein response (UPR) pathway is known to be activated in all cells [53]. Therefore, we investigated whether ER stress and concomitant UPR activation plays any role in sub-lethal HHcy induced endothelial dysfunction as well. Western blot analysis revealed that sub-lethal Hcy treatment causes activation of ER stress-associated UPR as evident by significant induction of three well known markers, namely, early UPR regulator protein GRP78, UPR transducer phosphorylated IRE1 (IRE1p) and UPR effector protein ATF4. An unresolved or sustained UPR may induce apoptosis majorly through induction of CHOP [54]. Interestingly, we detected no significant change in the expression level of CHOP upon exposure to sub-lethal HHcy (Figure 5A). Thus, we found that sub-lethal HHcy induces ER stress and concurrently activates adaptive UPR which does not lead to endothelial apoptosis. Thereafter, we hypothesized that ER stress-associated adaptive UPR activation is the sole cause of sub-lethal HHcy induced endothelial migration and proliferation defects. To explore this possibility, we used 4-PBA and TUDCA, two commonly used chemical chaperones with well known ER stress reducing properties [55]. Firstly, we confirmed alleviation of ER stress by reduction in the aberrant increase of GRP78 in case of both of the chemical chaperones (Figure S3A and S3B). Subsequently, through scratch wound assay we discovered that pre-treatment with 4-PBA and TUDCA could significantly rescue sub-lethal Hcy induced impaired endothelial migration (Figure 5B-5C and S3C-3D). Since migration of endothelial cells involves specific cytoplasmic changes that depend on remodeling of the actin cytoskeleton [56,57], we then carried out rhodamine phalloidin based F-actin staining to understand the basis of migratory abnormality in Hyperhomocysteinemic endothelial cells. As shown in the representative confocal images, we observed that when subjected to 2 mM Hcy treatment for 24 hours, endothelial cells exhibited abnormally elongated morphology which was reversed by 4-PBA pre-treatment (Figure 5D). Quantification of cellular aspect ratio confirmed that 4-PBA rescued aberrant elongation in Hyperhomocysteinemic cells (Figure 5E). On the contrary, endothelial cells with sub-lethal HHcy showed significant reduction of cellular surface area indicating that cytoplasm of these cells has

Preprints (www.preprints.org) | NOT PEER-REVIEWED | Posted: 5 September 2023 doi:10.20944/preprints202309.0215.v1

shrunk and similar to abnormal elongation, this anomaly was also rescued by 4-PBA (Figure 5D and 5F). Apart from differences in cell morphology, we also noticed that formation of actin stress fibers, which is associated with migratory force generation, were hampered in sub-lethal Hcy treated endothelial cells and 4-PBA pre-treatment caused their reappearance (Figure 5D). Taken together, the above-mentioned data indicates that sub-lethal Hcy induced adaptive UPR controls endothelial migration defect through aberrant remodeling of the actin cytoskeleton. However, as demonstrated by BrdU incorporation assay, we found that sub-lethal Hcy induced impaired endothelial proliferation did not improve after pre-treatment with 4-PBA and TUDCA (Figure 5G and S3E). This depicts that adaptive UPR activation influences only the migratory part of sub-lethal HHcy-associated endothelial dysfunction.

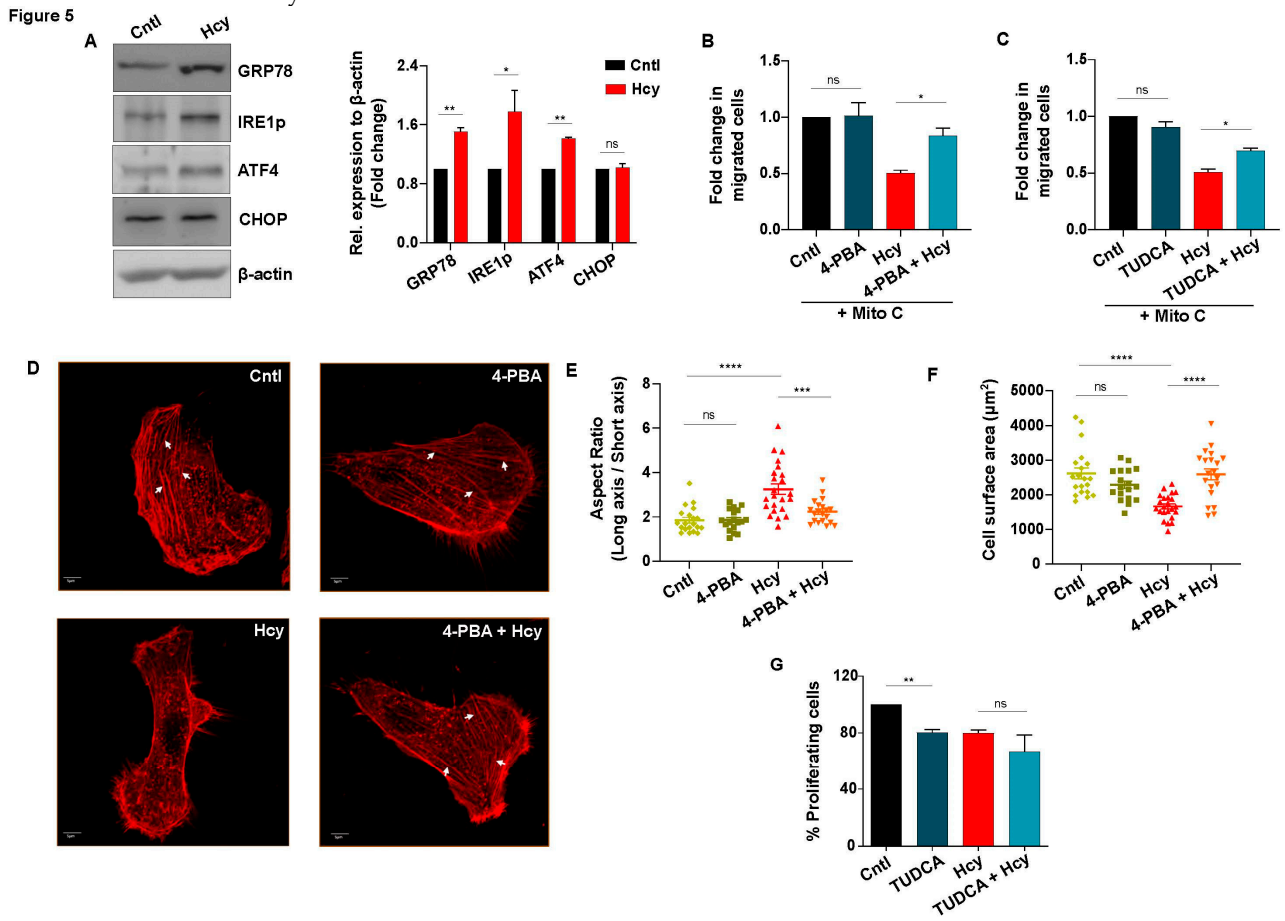

Figure 5. Sub-lethal HHcy induced adaptive UPR controls endothelial migration defect. (A) Representative western blots showing protein levels of UPR markers GRP78, IRE1p and ATF4 are upregulated upon 2 mM Hcy treatment for 24 h. Terminal UPR marker CHOP remained unaltered post sub-lethal Hcy treatment. As a loading control β-actin was used. Corresponding bar graph showing densitometric analysis (normalized to β-actin) of the blots. (B) & (C) Respective quantifications of scratch wound assay at 24 h revealing that chemical chaperone 4-PBA (1 mM) and TUDCA (1 mM) can significantly improve sub-lethal HHcy induced endothelial migration defect. (D) Representative confocal images of rhodamine-phalloidin stained endothelial cells showing that sub-lethal Hcy induced abnormally elongated cell morphology as well as actin stress fiber (white arrows) disappearance are rescued by 4-PBA pre-treatment. Scale bar, 5 μm. (E) ImageJ based analysis demonstrating that 4-PBA pre-treatment reversed the aberrant reduction in cellular aspect ratio (major axis / minor axis), induced by 24 h treatment of 2 mM Hcy. (F) Quantification by ImageJ suggesting that exposure to sub-lethal Hcy significantly decreased the surface area of endothelial cells which was rescued by 4-PBA. (G) Bar plot showing no beneficial effect of chemical chaperone TUDCA on impairment of endothelial proliferation caused by sub-lethal Hcy treatment. Data are shown as Mean±SEM with n ≥ 3. *P≤0.05, **P≤0.01, ***P≤0.001, ****P≤0.0001 and ns is non-significant (P>0.05).

 doi:10.20944/preprints202309.0215.v1

3.6. Sub-lethal HHcy linked malfunctioned ETC causes reduction of mitochondrial respiration, a crucial regulator of endothelial proliferation

Cellular metabolism is a primary mechanism that governs endothelial proliferation [34,35]. Since HHcy itself is a metabolic disorder, we wanted to study its impact on mitochondrial respiration and glycolysis, two major components of endothelial metabolism. Using an extracellular metabolic flux analyzer we found that oxygen consumption rate (OCR) is drastically reduced in sub-lethal Hcy treated endothelial cells (Figure 6A). Basal respiration, ATP production and maximal respiration, analyzed by measurement of area under the curve (AUC), were decreased by around 40-50% which dictates severe impairment of mitochondrial respiration in endothelial cells exposed to non-cytotoxic concentration of Hcy (Figure 6B-6D). Our next goal was to determine whether along with mitochondrial respiration, sub-lethal HHcy also influences overall mitochondrial function and integrity. Measurement of mitochondrial membrane potential using potentiometric fluorescent dye TMRE showed no significant change in Hyperhomocysteinemic endothelial cells as compared to untreated control ones (Figure S4A). Next, analysis of mitochondrial network integrity in mitoGFP transduced cells demonstrated absence of any observable mitochondrial fragmentation and overall mitochondrial network also seemed to be unaltered upon induction of sub-lethal HHcy in endothelial cells (Figure S4B). ImageJ based quantification of mitochondrial length further ascertained no significant change of mitochondrial morphology in Hyperhomocysteinemic endothelial cells (Figure S4C). Together, we demonstrated that while Hcy can impair mitochondrial respiration at a non-cytotoxic level, overall mitochondrial integrity and health remained unaltered. ER stress by influencing mitochondrial function is known to cause pathological abnormalities in several diseases [58,59]. So, our next objective was to check whether sub-lethal HHcy induced endothelial mitochondrial respiration defect is a consequence of ER stress-associated adaptive UPR activation. As elucidated by OCR curves and adjoining quantifications, pre-treatment with chemical chaperone TUDCA failed to improve the decrease in mitochondrial respiratory parameters in presence of sub-lethal HHcy (Figure 6E-6H). Another chemical chaperone, 4-PBA, produced a similar result (Figure S4D-S4G). This demonstrates that adaptive UPR is not causal to sub-lethal HHcy induced endothelial mitochondrial respiration defect. Next, through targeted metabolomics of TCA cycle metabolites we found that sub-lethal Hcy exposure did not cause suppression of TCA cycle either (Figure 6I). Thus, after nullifying ER stress and TCA cycle impairment, we looked into the status of mitochondrial bioenergetics to find out the source of mitochondrial respiration defect involved in sub-lethal HHcy associated endothelial dysfunction. Measurement of cytochrome C oxidase (COX) activity confirmed that sub-lethal HHcy induced a 40% reduction in the functionality of endothelial mitochondria's terminal electron acceptor (Figure 6J). Collectively, we demonstrated that despite not affecting overall mitochondrial health, sub-lethally increased Hcy impairs endothelial mitochondrial respiration which happens due to a dysfunctional electron transport chain.

Preprints (www.preprints.org) | NOT PEER-REVIEWED | Posted: 5 September 2023 doi:10.20944/preprints202309.0215.v1

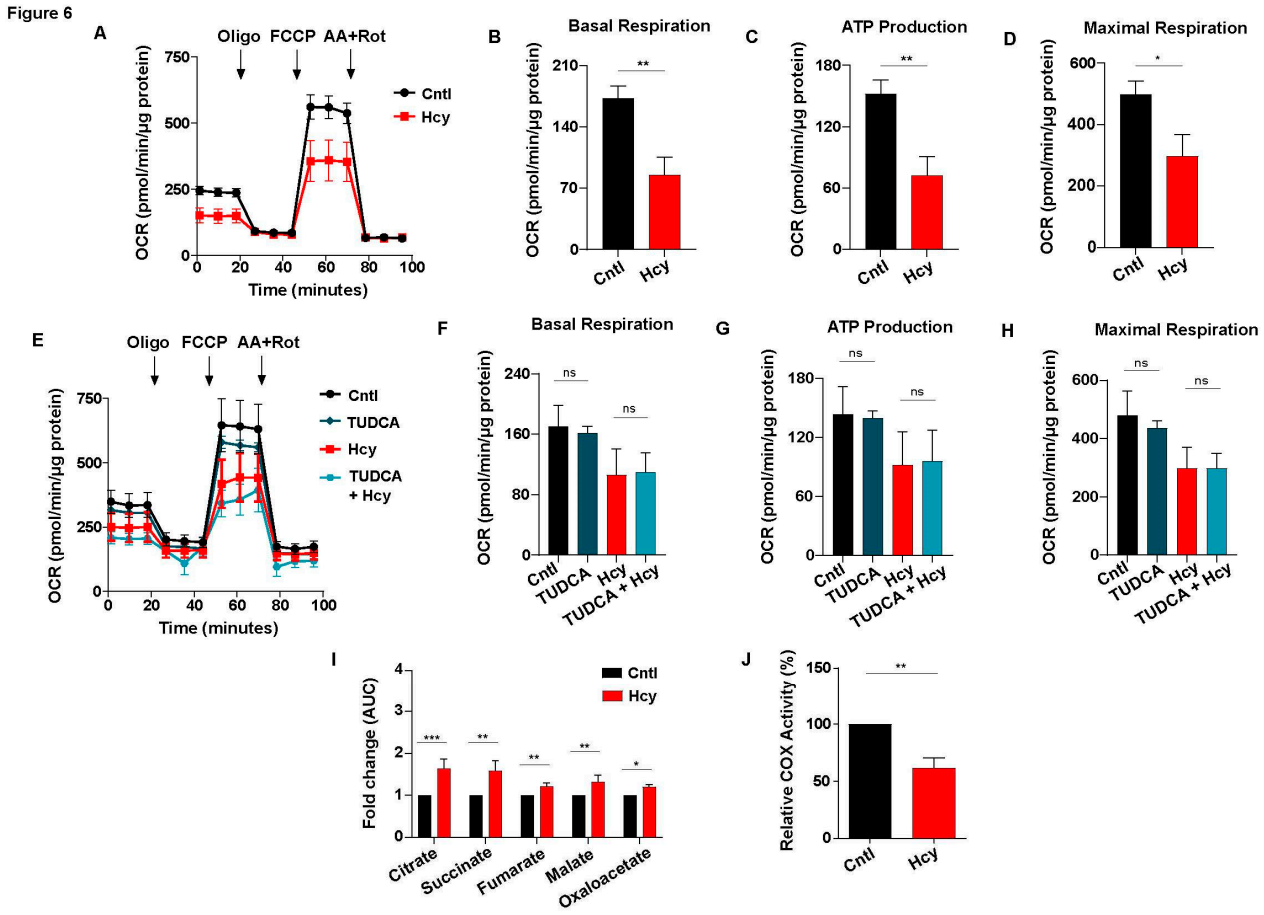

Figure 6. Sub-lethal HHcy linked malfunctional ETC impairs mitochondrial respiration of endothelial cells. (**A**) OCR curves showing drastic reduction of endothelial mitochondrial respiration upon 2 mM Hcy treatment for 24 h as measured by an extracellular flux analyzer. (**B**), (**C**) & (**D**) Respective bar graphs demonstrating that in comparison to untreated cells, there is significant decrease in basal respiration, ATP production and maximal respiration of endothelial cells with sub-lethal HHcy. (**E**) OCR curves showing no restoration of sub-lethal HHcy induced mitochondrial respiration defect in presence of TUDCA. (**F**), (**G**) & (**H**) Bar plots respectively showing no significant improvement in the reduction of basal respiration, ATP production and maximal respiration upon TUDCA pre-treatment, as compared to sub-lethal Hcy treated endothelial cells. (**I**) Targeted metabolomics mediated quantification exhibiting significant elevation of metabolites of TCA cycle in sub-lethal Hcy treated endothelial cells compared to untreated control cells. AUC, area under the curve. (**J**) Bar plot showing that sub-lethal HHcy in endothelial cells causes significant reduction in enzymatic activity of COX, the terminal electron acceptor of ETC. Data are shown as Mean±SEM with n ≥ 3. *P≤0.05, **P≤0.01, ***P≤0.001 and ns is non-significant (P>0.05). .

3.7. Endothelial glycolysis is elevated upon sub-lethal HHcy mediated mitochondrial respiration defect

Impairment of mitochondrial respiration is known to elevate endothelial glycolysis [34]. As there was a substantial loss of ATP level, we speculated that exposure to sub-lethal dose of Hcy will also increase endothelial glycolysis. Indeed, analysis of extracellular acidification rate (ECAR) showed that glycolysis has sharply increased in Hyperhomocysteinemic endothelial cells (Figure 7A). Quantification of basal glycolysis, glycolytic reserve and glycolytic capacity also revealed that sub-lethal Hcy treated cells had significantly higher levels of these parameters of glycolytic metabolism as compared to untreated control cells (Figure 7B-7D). To verify this, we analyzed the levels of glycolytic metabolites through targeted metabolomics. In line with our extracellular flux analysis, all the glycolytic intermediates of endothelial cells were found to be significantly elevated upon 2 mM Hcy treatment for 24 hours (Figure 7E). To further confirm, we assessed glucose consumption using

Preprints (www.preprints.org) | NOT PEER-REVIEWED | Posted: 5 September 2023 doi:10.20944/preprints202309.0215.v1

the fluorescent analog 2-NBDG which established a significantly higher uptake of extracellular glucose in sub-lethal Hcy treated endothelial cells (Figure 7F). Overall, we found that sub-lethal HHcy increases endothelial glycolysis probably to cope with abolished mitochondrial respiration.

Figure 7

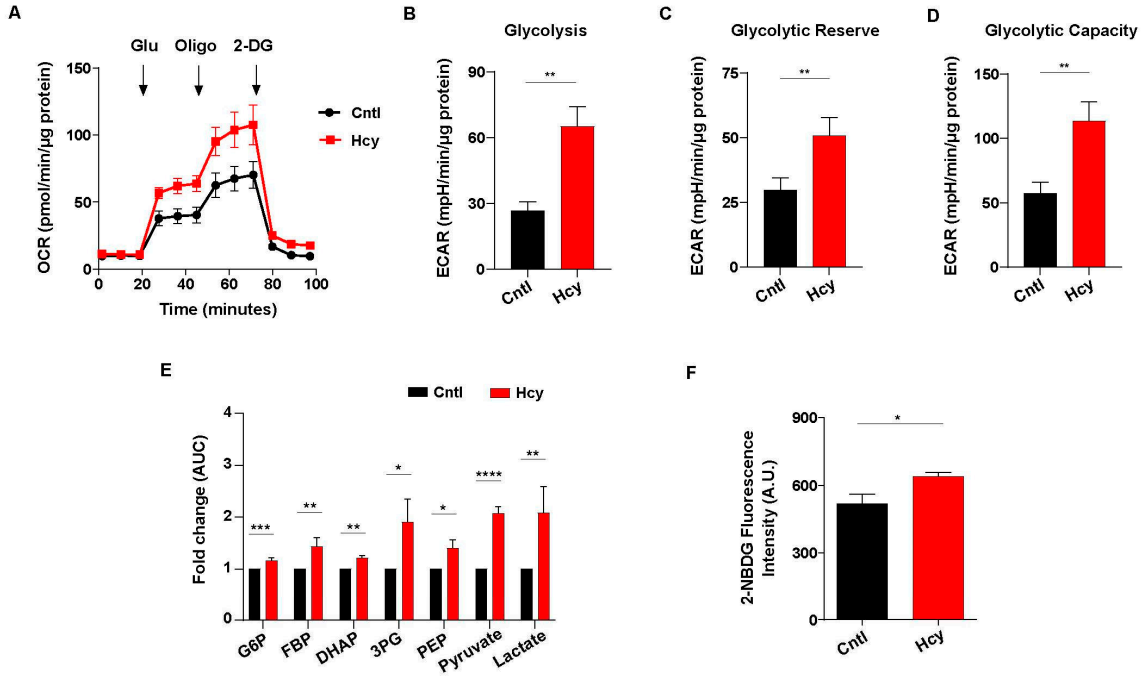

Figure 7. Glycolysis is elevated upon induction of sub-lethal HHcy in endothelial cells. (**A**) ECAR curves showing drastically upregulated glycolysis of endothelial cells treated by 2 mM Hcy for 24 h as measured by an extracellular flux analyzer. (**B**), (**C**) & (**D**) Respective bar graphs revealing that in comparison to untreated cells, there is a significant enhancement of glycolysis, glycolytic reserve and glycolytic capacity of sub-lethal Hcy treated endothelial cells. (**E**) Bar graph of targeted metabolomics showing metabolic intermediates of glycolysis are elevated in endothelial cells with sub-lethal HHcy. AUC, area under the curve. (**F**) Glucose uptake assay using fluorescence analog 2-NBDG showing that in comparison to control cells, consumption of extracellular glucose is higher in sub-lethal Hcy treated endothelial cells. Data are shown as Mean±SEM with n ≥ 3. *P≤0.05, **P≤0.01, ***P≤0.001, and ****P≤0.0001.

3.8. Mechanistic signatures of moderate HHcy are conserved in adult endothelial cells

Primary and immortalized HUVEC which were used for this study are cellular models of neonatal origin. To check whether adult endothelial cells will respond similarly to a pathologically relevant dose of Hcy, we analyzed an available microarray dataset (GSE175735) from Gene Expression Omnibus (GEO) in which adult origin primary human aortic endothelial cells (HAEC) were exposed to a sub-millimolar concentration of Hcy treatment for 48 hours [42] (Figure 8A). Our analysis revealed that several genes involved in cellular migration and cell cycle were significantly downregulated upon Hcy treatment (Figure 8B). However, affirming our previously mentioned *in vitro* and *in vivo* observations, genes associated with angiogenic growth factor signaling showed absence of a trend of downregulation in the Hcy treated group as compared to the control group. Similarly, a trend of upregulation was observed in several genes associated with cellular antioxidant defense systems suggesting a possible aversion of oxidative stress even in sub-millimolar Hcy treated adult endothelial cells (Figure 8C). Furthermore, we found that a number of genes which belong to

Preprints (www.preprints.org) | NOT PEER-REVIEWED | Posted: 5 September 2023 doi:10.20944/preprints202309.0215.v1

UPR are also significantly upregulated in Hyperhomocysteinemic HAEC cells (Figure 8D). To gain insight into cellular metabolism, we then checked differentially altered genetic markers of TCA cycle and glycolysis and observed that in corroboration to our metabolic study, not only TCA cycle but also several markers of glycolysis were exhibiting an upregulated trend upon Hcy treatment (Figure 8E). Overall, as shown in the heat maps, our analysis established that the characteristics of pathological HHcy induced functional impairments through UPR activation and metabolic alteration, are conserved even in adult endothelial cells.

Figure 8

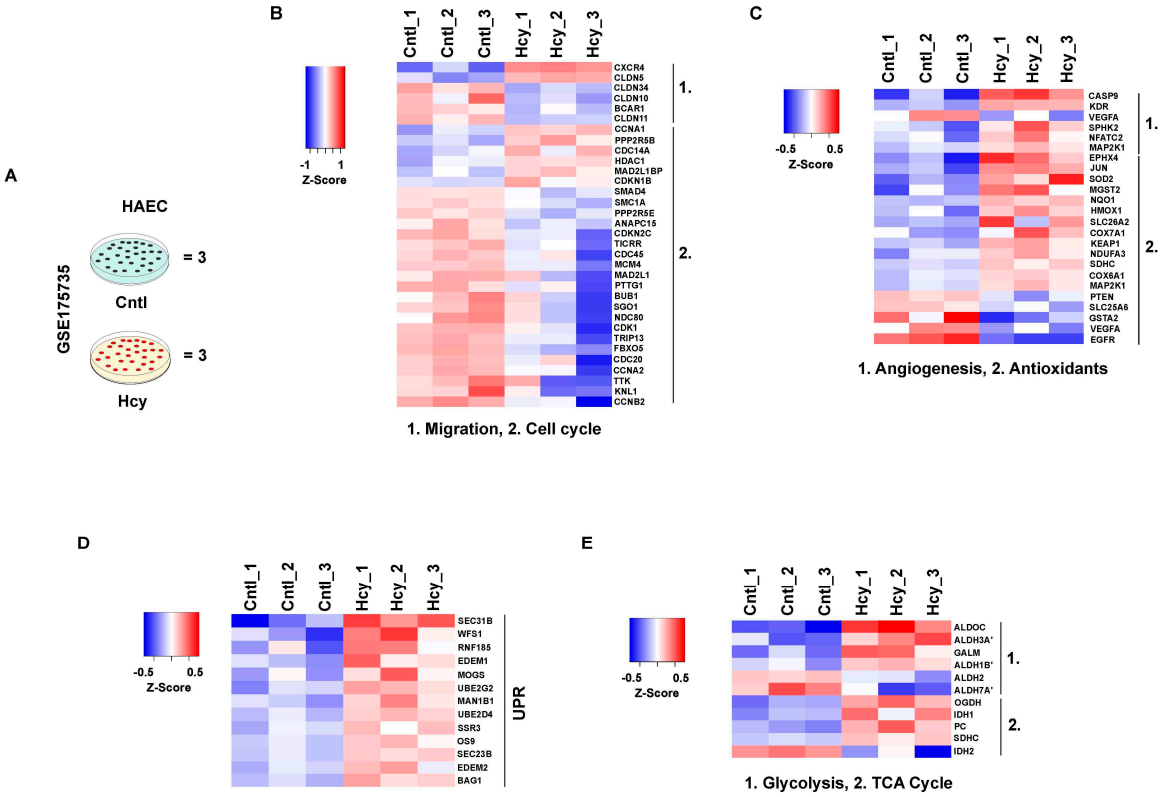

Figure 8. Mechanistic features of pathologically relevant Hcy exposure are conserved in adult endothelial cells. (**A**) Schematic diagram showing experimental model and treatment condition used for microarray profiling of GSE175735 from GEO database. (**B**) Heatmap illustrating the trend of downregulation in differentially expressed genes (DEGs) of cell cycle and cellular migration as compared between control and Hcy treated groups. (**C**), (**D**) & (**E**) Respective heatmaps showing pathway specific expression of angiogenesis and antioxidant response genes, UPR and metabolism (TCA cycle and glycolysis), in the same Hcy treated and untreated control cell groups. Statistically significant (p-value < 0.05) genes were considered to obtain DEGs. Respective color legends representing Z-score ((observed value - mean) / standard deviation) values. 3 sets of samples each from control and Hcy treated cells were used for analysis. .

4. Discussion

Endothelial cells constitute the innermost layer of blood vessels and are essential for angiogenesis, a tightly regulated multistep process involving cellular migration and proliferation [60]. Although a large number of clinical and experimental studies have linked HHcy to vascular endothelial dysfunction, it is still not clear whether this association is causal or consequential [61–63]. Moreover, serum Hcy lowering through vitamin B supplements in patients with cardiovascular complications, did not produce encouraging results [64,65]. This in turn suggests that there might be subtle functional changes in Hyperhomocysteinemic endothelial cells that need attention. In this regard, most of the previous cell based studies focused on severely elevated Hcy mediated

endothelial cytotoxicity [7–9]. Due to the fact that severe HHcy which is induced by inborn error in Hcy catabolism [45], a rare clinical condition, our aim in this study was to explore the mechanistic basis of how moderate HHcy affects endothelial function in the absence of cell death. For this purpose, we induced HHcy exogenously and generated moderate Hyperhomocysteinemic condition in endothelial cells with no detectable cytotoxicity. Using this model system we found that even at a non-cytotoxic level, Hcy can cause endothelial dysfunction. Further, our data suggested that sub-lethal increase in Hcy levels can impair endothelial migration and proliferation, two critical components of endothelial function required during angiogenesis. This anti-migratory and anti-proliferative effect of Hcy on endothelial cells was in line with previous studies [22,23,66]. Of note, it can be mentioned here that the effect of HHcy on cellular migration and proliferation might be specific to only the endothelium component of the vasculature as several previous findings suggested an opposite trend in Hyperhomocysteinemic vascular smooth muscle cells [67–69]. The role of canonical VEGF/VEGFR signaling in the context of HHcy induced endothelial migration and proliferation impairment was controversial [26–28]. In our sub-lethal Hcy treated endothelial cells we found that the expression levels of canonical VEGF/VEGFR signaling markers are not suppressed. Moreover, previous reports suggested that oxidative stress play a pivotal role in inducing cell death in Hyperhomocysteinemic endothelial cells [9,10]. However, we found that moderate HHcy-induced endothelial dysfunction is not associated with oxidative stress.

Previous research using mammalian model systems of mice [70,71], rats [72,73] and even monkeys [74] had shown that diet induced HHcy can detrimentally influence the vascular endothelium. Dietary modulations, though, could have a potential confounding effect on these model systems. On the other hand, CBS KO mouse models of genetically induced severe HHcy exhibited growth retardation and neonatal lethality, but unlike humans, vascular abnormality is not the primary cause of their deaths [6,70]. Furthermore, use of different methods to generate HHcy in animal studies have created inconsistencies in the cardiovascular phenotype and moderate HHcy-associated most common vascular complications like atherosclerosis and thrombosis have never been spontaneously recapitulated in these animal models [70]. As Zebrafish is widely used in modelling cardiovascular research [75], in order to understand whether moderate HHcy can cause vascular abnormality in an animal model also, we have generated a zebrafish model of sub-lethal HHcy by targeting CBS. Using this zebrafish model we found that although sub-lethal HHcy does not influence initial vascular development and viability of the organisms, subtle functional events like angiogenesis of CVP and ISV formation is impaired. BMP signaling is known to play a crucial role in CVP formation while ISV formation is regulated by VEGF signaling [76]. This suggests that any specifically altered growth factor signaling may not be the sole cause of sub-lethal HHcy induced vascular endothelial dysfunction. In a previous study, Lee et al also reported that exposure to Hcy containing water can induce vascular dysfunction in larval zebrafish [77]. A recent study with a knockout model of HHcy also showed a similar abnormality in ISV formation of zebrafish [78]. Further, to check the specificity of moderate HHcy induced vascular abnormality *in vivo*, we also generated a viable zebrafish model of CGL deficiency as control. In humans, CGL deficiency is associated with urinary excretion of excess Cystathionine and may induce cognitive impairment [47]. In this study, we revealed that CGL knockdown does not induce any vascular abnormality which demonstrates that sub-lethal HHcy induced vascular endothelial dysfunction is not due to an alteration of the transsulfuration pathway *per se*. It is worth mentioning here that unlike CBS KO mice, CGL deficient mice are viable and also do not exhibit any phenotype under normal condition [79]. Lastly, in the line of our cellular data, we found that sub-lethal HHcy induced vascular endothelial dysfunction in zebrafish is not associated with suppressed VEGF/VEGFR signaling and oxidative stress generation.

Hcy is regarded as a potent inducer of ER-stress in not only endothelial cells [13,14,16,50] but also in other cell types [51,52]; However, it should be emphasized here that most of the previous studies have connected Hcy-induced ER-stress to apoptotic cell death. Our data revealed that at a non-cytotoxic level also, Hcy can induce ER-stress in endothelial cells but it subsequently activates an adaptive UPR that is not terminal in nature and may not necessarily induce cell death. Subsequently by blocking ER-stress using chemical chaperones, we unveiled for the first time that in

 doi:10.20944/preprints202309.0215.v1

between migration and proliferation defects, sub-lethal Hcy induced adaptive UPR controls only the migratory axis. Here to mention that the chemical chaperones, 4-PBA and TUDCA, which were used in our study, have immense therapeutic potential and produced encouraging results in several clinical trials [80,81]. Being specialized epithelial cells, remodeling of the actin cytoskeleton is absolutely essential for amoeboid migration of endothelial cells [57]. For instance, Stroka et al. suggested that upon TNFα treatment, endothelial cells can rapidly undergo cytoskeletal rearrangement and become elongated which ultimately reduces their migration time [82]. Our results confirmed that a similar aberrant modulation of actin cytoskeleton leading to abnormal cell elongation is the mechanistic basis through which ER-stress exerts its anti-migratory effect on endothelial cells in moderate HHcy. Previous reports showed that the proteins of the UPR pathways are linked to actin dynamics in other cell types [83,84] which further support our conclusion that adaptive UPR plays an upstream signal to control aberrant cytoskeletal dynamics in endothelial cells that explains their altered migratory phenotype in moderate HHcy.

One of the major determinants of cellular proliferation is metabolism [85]. Particularly, in endothelial cells, latest research in this aspect suggests that disruption of specific metabolic pathways can impair their proliferation without influencing migratory property [34,35]. Metabolic reprogramming of vascular endothelial cells has also emerged as a novel therapeutic target for pathological angiogenesis in recent years [86,87]. Nevertheless, the regulation of endothelial metabolism in HHcy remains largely unexplored. Our study elucidates that at a sub-lethal level, Hcy can inhibit mitochondrial respiration in endothelial cells. In contrast to previously published data, we revealed that sub-lethal HHcy induced impairment of mitochondrial respiration, may not inevitably cause alteration of mitochondrial membrane potential and fragmentation of mitochondrial network. Diebold et al. reported a similar outcome when endothelial cells were treated with antimycin A, a well-known mitochondrial complex III blocker [34]. ER stress can crosstalk with mitochondria and thereby influence energy metabolism, cell survival and protein folding which may induce pleiotropic consequences on various diseases like neurodegenerative and lysosomal storage disorders [58,59,88]. However, we observed that mitochondrial respiration defect in moderate HHcy, as assessed in the presence of chemical chaperones, is not a consequence of ER stress-associated adaptive UPR. Our data also suggested that both glycolysis and TCA cycle are upregulated in moderate HHcy. Owing to the fact that TCA cycle intermediates also have anaplerotic roles and can act as precursor for amino acids, fatty acids and nucleotides [89]; the role of TCA cycle metabolites in Hyperhomocysteinemic endothelial cells remains an exciting open question. As TCA Cycle which feeds reducing equivalents to mitochondrial respiratory chain, is not repressed upon induction of moderate HHcy in endothelial cells we narrowed down that the electron transport chain itself might be malfunctioning. Indeed we found that sub-lethal HHcy causes a reduction in the enzymatic activity of COX, the complex IV of ETC. These results are in support of recent observations where complex III and IV deficiency mediated impairment of mitochondrial respiration was reported to be necessary for endothelial function in developmental as well as pathological angiogenesis [34]. In addition to endothelial cells, HHcy is also reported to cause significant inhibition of complex II, III and IV in isolated rat cardiac mitochondria [90]. It will therefore be interesting to conduct further research focusing on in-depth understanding of the mitochondrial bioenergetics status and its alteration in Hyperhomocysteinemic endothelial cells. Beside mitochondrial respiration, glycolysis also plays a vital role in endothelial cells and its complete suppression can induce cell death [91]. In accordance, our data demonstrated that moderate HHcy rewires glycolysis by upregulating it and that is probably a prerequisite for survival of endothelial cells with compromised mitochondrial respiration in this stressed condition.

Endothelial dysfunction is regarded as an important contributor to the pathobiology of atherosclerosis [92] which is a disease of the adult vasculature. Since fetal tissue derived HUVEC cell line may not fully represent the mature endothelium of the adult vasculature, we used an existing microarray dataset [42] of adult endothelial cells exposed to pathologically relevant Hcy doses. Our gene expression analysis established that all the mechanistic signatures and processes elucidated by

us in moderate HHcy are conserved even in endothelial cells of adult origin and that further endorse our experimental observations.

In conclusion, the findings of our work elucidates that in absence of lethality, moderate HHcy can cause endothelial dysfunction by altering their migration and proliferation capacities. Mechanistically, an independent bimodal regulation through adaptive UPR activation and metabolic rewiring act as the upstream cues to generate these defects and that may later on increase the risk of developing vascular diseases. Our results also give a clue that in contrast to severe HHcy-induced early lethality, the aged or nutritionally deficient population of mild to moderate HHcy are clinically vulnerable to the development of cardiovascular diseases with time.

Author Contributions: B.C. performed most of the experiments, compiled and analyzed the data and wrote the primary draft of the manuscript. F.F. and S.S. performed experiments and data analysis. S.S.R. conceptualized the idea, provided the resources, wrote the final manuscript and supervised the overall research. All the authors have read the manuscript and agreed to communicate for the publication.

Funding: S.S.R. received the funding for this work from the Council of Scientific and Industrial Research (CSIR), India through the research grant (CardioMed-BSC0122). B.C. was supported through a research fellowship from Indian Council of Medical Research (ICMR), India. S.S. receives a research fellowship from Council of Scientific and Industrial Research (CSIR), India.

Data Availability Statement: The transcriptome dataset analyzed in the current study has been previously published by Jan M et al. (2021) [40] and is available at the NCBI Gene Expression Omnibus (accession no. GSE175735). https://www.ncbi.nlm.nih.gov/geo/query/acc.cgi.

Acknowledgments: We thank the Core Imaging Facility of CSIR - IGIB and Ms. Vandana Singh, Dr. Dilip Menon and Dr. Samatha Mathew for their technical assistance during confocal microscopy. We are also grateful to Dr. Sridhar Sivasubbu for providing us the transgenic zebrafish model and coordinating the maintenance of Institutional Zebrafish Facility. We also thank Dr. Paras Sehgal and Mr. Gyan Ranjan for helping with zebrafish embryos. The authors also acknowledge the technical help from Ms. Saumya Johri for Seahorse extracellular flux analysis and Mr. Praveen Singh and Ms. Mamta Rathore for HPLC measurements. The authors also thank Lakshita Sharma for helping in metabolomics analysis.

Disclosure Statement: The authors declare no conflict of interest.

Ethical disclosure: All experiments on zebrafish were performed in accordance with the guidelines of Institutional Animal Ethics Committee (IAEC), CSIR - Institute of Genomics & Integrative Biology. No human research participants were used in this study.

References

1. Zaric BL, Obradovic M, Bajic V, Haidara MA, Jovanovic M, Isenovic ER. Homocysteine and Hyperhomocysteinaemia. Curr Med Chem. 2019;26: 2948–2961.
2. Ganguly P, Alam SF. Role of homocysteine in the development of cardiovascular disease. Nutr J. 2015;14: 6.
3. Troen AM. The central nervous system in animal models of hyperhomocysteinemia. Prog Neuropsychopharmacol Biol Psychiatry. 2005;29: 1140–1151.
4. Tinelli C, Di Pino A, Ficulle E, Marcelli S, Feligioni M. Hyperhomocysteinemia as a Risk Factor and Potential Nutraceutical Target for Certain Pathologies. Front Nutr. 2019;6: 49.
5. McCully KS. Vascular pathology of homocysteinemia: implications for the pathogenesis of arteriosclerosis. Am J Pathol. 1969;56: 111–128.
6. Kruger WD. Cystathionine β-synthase deficiency: Of mice and men. Mol Genet Metab. 2017;121: 199–205.
7. Cui S, Li W, Wang P, Lv X, Gao Y, Huang G. Folic acid inhibits homocysteine-induced cell apoptosis in human umbilical vein endothelial cells. Mol Cell Biochem. 2018;444: 77–86.
8. Suhara T, Fukuo K, Yasuda O, Tsubakimoto M, Takemura Y, Kawamoto H, et al. Homocysteine enhances endothelial apoptosis via upregulation of Fas-mediated pathways. Hypertension. 2004;43: 1208–1213.
9. Tian X, Zhao L, Song X, Yan Y, Liu N, Li T, et al. HSP27 Inhibits Homocysteine-Induced Endothelial Apoptosis by Modulation of ROS Production and Mitochondrial Caspase-Dependent Apoptotic Pathway. Biomed Res Int. 2016;2016: 4847874.
10. Liu S, Sun Z, Chu P, Li H, Ahsan A, Zhou Z, et al. EGCG protects against homocysteine-induced human umbilical vein endothelial cells apoptosis by modulating mitochondrial-dependent apoptotic signaling and PI3K/Akt/eNOS signaling pathways. Apoptosis. 2017;22: 672–680.

11. Gomez J, Sanchez-Roman I, Gomez A, Sanchez C, Suarez H, Lopez-Torres M, et al. Methionine and homocysteine modulate the rate of ROS generation of isolated mitochondria in vitro. J Bioenerg Biomembr. 2011;43: 377–386.
12. Outinen PA, Sood SK, Liaw PC, Sarge KD, Maeda N, Hirsh J, et al. Characterization of the stress-inducing effects of homocysteine. Biochem J. 1998;332 (Pt 1): 213–221.
13. Zhang Z, Wei C, Zhou Y, Yan T, Wang Z, Li W, et al. Homocysteine Induces Apoptosis of Human Umbilical Vein Endothelial Cells via Mitochondrial Dysfunction and Endoplasmic Reticulum Stress. Oxid Med Cell Longev. 2017;2017: 5736506.
14. Kil J-S, Jeong S-O, Chung H-T, Pae H-O. Piceatannol attenuates homocysteine-induced endoplasmic reticulum stress and endothelial cell damage via heme oxygenase-1 expression. Amino Acids. 2017;49: 735–745.
15. Hu H, Wang C, Jin Y, Meng Q, Liu Q, Liu Z, et al. Catalpol Inhibits Homocysteine-induced Oxidation and Inflammation via Inhibiting Nox4/NF-κB and GRP78/PERK Pathways in Human Aorta Endothelial Cells. Inflammation. 2019;42: 64–80.
16. Ji C, Yi H, Huang J, Zhang W, Zheng M. Propofol alleviates inflammation and apoptosis in HCY-induced HUVECs by inhibiting endoplasmic reticulum stress. Mol Med Rep. 2021;23. doi:10.3892/mmr.2021.11972
17. Guéant J-L, Guéant-Rodriguez R-M, Oussalah A, Zuily S, Rosenberg I. Hyperhomocysteinemia in Cardiovascular Diseases: Revisiting Observational Studies and Clinical Trials. Thromb Haemost. 2023;123: 270–282.
18. Guieu R, Ruf J, Mottola G. Hyperhomocysteinemia and cardiovascular diseases. Ann Biol Clin . 2022;80: 7–14.
19. Abhinand CS, Raju R, Soumya SJ, Arya PS, Sudhakaran PR. VEGF-A/VEGFR2 signaling network in endothelial cells relevant to angiogenesis. J Cell Commun Signal. 2016;10: 347–354.
20. Homocysteine Inhibits Angiogenesis in Vitro and in Vivo. Biochem Biophys Res Commun. 2001;281: 726–731.
21. Duan J, Murohara T, Ikeda H, Sasaki K, Shintani S, Akita T, et al. Hyperhomocysteinemia impairs angiogenesis in response to hindlimb ischemia. Arterioscler Thromb Vasc Biol. 2000;20: 2579–2585.
22. Chang P-Y, Lu S-C, Lee C-M, Chen Y-J, Dugan TA, Huang W-H, et al. Homocysteine inhibits arterial endothelial cell growth through transcriptional downregulation of fibroblast growth factor-2 involving G protein and DNA methylation. Circ Res. 2008;102: 933–941.
23. Yu J, Zhang L-L, Wu X-P, Zhao R, Meng Z-X, Wang K, et al. Homocysteine inhibits the viability and migration ability of human umbilical vein endothelial cells by downregulating the expression of vascular endothelial growth factor. Exp Ther Med. 2019;18: 3913–3919.
24. Rodríguez-Nieto S, Chavarría T, Martínez-Poveda B, Sánchez-Jiménez F, Rodríguez Quesada A, Medina MA. Anti-angiogenic effects of homocysteine on cultured endothelial cells. Biochem Biophys Res Commun. 2002;293: 497–500.
25. Saha S, Chakraborty PK, Xiong X, Dwivedi SKD, Mustafi SB, Leigh NR, et al. Cystathionine β-synthase regulates endothelial function via protein S-sulfhydration. FASEB J. 2016;30: 441–456.
26. Zhang Q, Li Q, Chen Y, Huang X, Yang IH, Cao L, et al. Homocysteine-impaired angiogenesis is associated with VEGF/VEGFR inhibition. Front Biosci . 2012;4: 2525–2535.
27. Shastry S, Tyagi N, Hayden MR, Tyagi SC. Proteomic analysis of homocysteine inhibition of microvascular endothelial cell angiogenesis. Cell Mol Biol . 2004;50: 931–937.
28. Roybal CN, Yang S, Sun C-W, Hurtado D, Vander Jagt DL, Townes TM, et al. Homocysteine increases the expression of vascular endothelial growth factor by a mechanism involving endoplasmic reticulum stress and transcription factor ATF4. J Biol Chem. 2004;279: 14844–14852.
29. Tawfik A, Markand S, Al-Shabrawey M, Mayo JN, Reynolds J, Bearden SE, et al. Alterations of retinal vasculature in cystathionine-β-synthase heterozygous mice: a model of mild to moderate hyperhomocysteinemia. Am J Pathol. 2014;184: 2573–2585.
30. Leung SWS, Shi Y. The glycolytic process in endothelial cells and its implications. Acta Pharmacol Sin. 2022;43: 251–259.
31. Bierhansl L, Conradi L-C, Treps L, Dewerchin M, Carmeliet P. Central Role of Metabolism in Endothelial Cell Function and Vascular Disease. Physiology . 2017;32: 126–140.
32. Goveia J, Stapor P, Carmeliet P. Principles of targeting endothelial cell metabolism to treat angiogenesis and endothelial cell dysfunction in disease. EMBO Mol Med. 2014;6: 1105–1120.
33. Deng J, Lü S, Liu H, Liu B, Jiang C, Xu Q, et al. Homocysteine Activates B Cells via Regulating PKM2-Dependent Metabolic Reprogramming. J Immunol. 2017;198: 170–183.
34. Diebold LP, Gil HJ, Gao P, Martinez CA, Weinberg SE, Chandel NS. Mitochondrial complex III is necessary for endothelial cell proliferation during angiogenesis. Nat Metab. 2019;1: 158–171.
35. Kim B, Li J, Jang C, Arany Z. Glutamine fuels proliferation but not migration of endothelial cells. EMBO J. 2017;36: 2321–2333.
36. McCully KS. Homocysteine and vascular disease. Nat Med. 1996;2: 386–389.

37. Lalwani MK, Sharma M, Singh AR, Chauhan RK, Patowary A, Singh N, et al. Reverse genetics screen in zebrafish identifies a role of miR-142a-3p in vascular development and integrity. PLoS One. 2012;7: e52588.
38. Rai A, Chatterjee B, Bhowmick S, Sagar S, Roy SS. Beclin 1 controls pigmentation by changing the nuclear localization of melanogenic factor MITF. Biochem Biophys Res Commun. 2020;528: 719–725.
39. Carpentier G, Berndt S, Ferratge S, Rasband W, Cuendet M, Uzan G, et al. Angiogenesis Analyzer for ImageJ - A comparative morphometric analysis of "Endothelial Tube Formation Assay" and "Fibrin Bead Assay." Sci Rep. 2020;10: 11568.
40. Sagar S, Faizan MI, Chaudhary N, Singh V, Singh P, Gheware A, et al. Obesity impairs cardiolipin-dependent mitophagy and therapeutic intercellular mitochondrial transfer ability of mesenchymal stem cells. Cell Death Dis. 2023;14: 324.
41. Faizan MI, Chaudhuri R, Sagar S, Albogami S, Chaudhary N, Azmi I, et al. NSP4 and ORF9b of SARS-CoV-2 Induce Pro-Inflammatory Mitochondrial DNA Release in Inner Membrane-Derived Vesicles. Cells. 2022;11. doi:10.3390/cells11192969
42. Jan M, Cueto R, Jiang X, Lu L, Sardy J, Xiong X, et al. Molecular processes mediating hyperhomocysteinemia-induced metabolic reprogramming, redox regulation and growth inhibition in endothelial cells. Redox Biol. 2021;45: 102018.
43. Ritchie ME, Phipson B, Wu D, Hu Y, Law CW, Shi W, et al. limma powers differential expression analyses for RNA-sequencing and microarray studies. Nucleic Acids Res. 2015;43: e47.
44. Selhub J. Homocysteine metabolism. Annu Rev Nutr. 1999;19: 217–246.
45. Mudd SH, Skovby F, Levy HL, Pettigrew KD, Wilcken B, Pyeritz RE, et al. The natural history of homocystinuria due to cystathionine beta-synthase deficiency. Am J Hum Genet. 1985;37: 1–31.
46. Kaur B, Sharma PK, Chatterjee B, Bissa B, Nattarayan V, Ramasamy S, Bhat A, Lal M, et al. Defective Quality Control Autophagy in Hyperhomocysteinemia promotes ER Stress and consequent Neuronal apoptosis through proteotoxicity. Cell Commun Signal (in press).
47. Pascal TA, Gaull GE, Beratis NG, Gillam BM, Tallan HH. Cystathionase deficiency: evidence for genetic heterogeneity in primary cystathioninuria. Pediatr Res. 1978;12: 125–133.
48. Gore AV, Monzo K, Cha YR, Pan W, Weinstein BM. Vascular development in the zebrafish. Cold Spring Harb Perspect Med. 2012;2: a006684.
49. Wang X-C, Sun W-T, Yu C-M, Pun S-H, Underwood MJ, He G-W, et al. ER stress mediates homocysteine-induced endothelial dysfunction: Modulation of IKCa and SKCa channels. Atherosclerosis. 2015;242: 191–198.
50. Wu X, Zhang L, Miao Y, Yang J, Wang X, Wang C-C, et al. Homocysteine causes vascular endothelial dysfunction by disrupting endoplasmic reticulum redox homeostasis. Redox Biol. 2019;20: 46–59.
51. Yu X, Lv J, Zhu Y, Duan L, Ma L. Homocysteine inhibits hepatocyte proliferation via endoplasmic reticulum stress. PLoS One. 2013;8: e54265.
52. Sun W, Zhou Y, Xue H, Hou H, He G, Yang Q. Endoplasmic reticulum stress mediates homocysteine-induced hypertrophy of cardiac cells through activation of cyclic nucleotide phosphodiesterase 1C. Acta Biochim Biophys Sin . 2022;54: 388–399.
53. Hetz C. The unfolded protein response: controlling cell fate decisions under ER stress and beyond. Nat Rev Mol Cell Biol. 2012;13: 89–102.
54. Zinszner H, Kuroda M, Wang X, Batchvarova N, Lightfoot RT, Remotti H, et al. CHOP is implicated in programmed cell death in response to impaired function of the endoplasmic reticulum. Genes Dev. 1998;12: 982–995.
55. Ozcan U, Yilmaz E, Ozcan L, Furuhashi M, Vaillancourt E, Smith RO, et al. Chemical chaperones reduce ER stress and restore glucose homeostasis in a mouse model of type 2 diabetes. Science. 2006;313: 1137–1140.
56. Schaks M, Giannone G, Rottner K. Actin dynamics in cell migration. Essays Biochem. 2019;63: 483–495.
57. Lamalice L, Le Boeuf F, Huot J. Endothelial cell migration during angiogenesis. Circ Res. 2007;100: 782–794.
58. Townsend LK, Brunetta HS, Mori MAS. Mitochondria-associated ER membranes in glucose homeostasis and insulin resistance. Am J Physiol Endocrinol Metab. 2020;319: E1053–E1060.
59. Markovinovic A, Greig J, Martín-Guerrero SM, Salam S, Paillusson S. Endoplasmic reticulum-mitochondria signaling in neurons and neurodegenerative diseases. J Cell Sci. 2022;135. doi:10.1242/jcs.248534
60. Muñoz-Chápuli R, Quesada AR, Angel Medina M. Angiogenesis and signal transduction in endothelial cells. Cell Mol Life Sci. 2004;61: 2224–2243.
61. Wierzbicki AS. Homocysteine and cardiovascular disease: a review of the evidence. Diab Vasc Dis Res. 2007;4: 143–150.
62. Cleophas TJ, Hornstra N, van Hoogstraten B, van der Meulen J. Homocysteine, a risk factor for coronary artery disease or not? A meta-analysis. Am J Cardiol. 2000;86: 1005–9, A8.
63. Smulders YM, Blom HJ. The homocysteine controversy. J Inherit Metab Dis. 2011;34: 93–99.

64. Toole JF, Malinow MR, Chambless LE, Spence JD, Pettigrew LC, Howard VJ, et al. Lowering homocysteine in patients with ischemic stroke to prevent recurrent stroke, myocardial infarction, and death: the Vitamin Intervention for Stroke Prevention (VISP) randomized controlled trial. JAMA. 2004;291: 565–575.
65. Bønaa KH, Njølstad I, Ueland PM, Schirmer H, Tverdal A, Steigen T, et al. Homocysteine lowering and cardiovascular events after acute myocardial infarction. N Engl J Med. 2006;354: 1578–1588.
66. Zou T, Liu W-J, Li S-D, Zhou W, Yang J-F, Zou C-G. TRB3 mediates homocysteine-induced inhibition of endothelial cell proliferation. J Cell Physiol. 2011;226: 2782–2789.
67. Chiang J-K, Sung M-L, Yu H-R, Chang H-I, Kuo H-C, Tsai T-C, et al. Homocysteine induces smooth muscle cell proliferation through differential regulation of cyclins A and D1 expression. J Cell Physiol. 2011;226: 1017–1026.
68. Tsai JC, Perrella MA, Yoshizumi M, Hsieh CM, Haber E, Schlegel R, et al. Promotion of vascular smooth muscle cell growth by homocysteine: a link to atherosclerosis. Proc Natl Acad Sci U S A. 1994;91: 6369–6373.
69. Jiang C, Zhang H, Zhang W, Kong W, Zhu Y, Zhang H, et al. Homocysteine promotes vascular smooth muscle cell migration by induction of the adipokine resistin. Am J Physiol Cell Physiol. 2009;297: C1466–76.
70. Dayal S, Lentz SR. Murine models of hyperhomocysteinemia and their vascular phenotypes. Arterioscler Thromb Vasc Biol. 2008;28: 1596–1605.
71. Tan H, Jiang X, Yang F, Li Z, Liao D, Trial J, et al. Hyperhomocysteinemia inhibits post-injury reendothelialization in mice. Cardiovasc Res. 2006;69: 253–262.
72. Morita H, Kurihara H, Yoshida S, Saito Y, Shindo T, Oh-Hashi Y, et al. Diet-induced hyperhomocysteinemia exacerbates neointima formation in rat carotid arteries after balloon injury. Circulation. 2001;103: 133–139.
73. Zhang R, Ma J, Xia M, Zhu H, Ling W. Mild hyperhomocysteinemia induced by feeding rats diets rich in methionine or deficient in folate promotes early atherosclerotic inflammatory processes. J Nutr. 2004;134: 825–830.
74. Böger RH, Bode-Böger SM, Sydow K, Heistad DD, Lentz SR. Plasma concentration of asymmetric dimethylarginine, an endogenous inhibitor of nitric oxide synthase, is elevated in monkeys with hyperhomocyst(e)inemia or hypercholesterolemia. Arterioscler Thromb Vasc Biol. 2000;20: 1557–1564.
75. Bowley G, Kugler E, Wilkinson R, Lawrie A, van Eeden F, Chico TJA, et al. Zebrafish as a tractable model of human cardiovascular disease. Br J Pharmacol. 2022;179: 900–917.
76. Eberlein J, Herdt L, Malchow J, Rittershaus A, Baumeister S, Helker CS. Molecular and Cellular Mechanisms of Vascular Development in Zebrafish. Life. 2021;11. doi:10.3390/life11101088
77. Lee SJ, Park SH, Chung JF, Choi W, Huh HK. Homocysteine-induced peripheral microcirculation dysfunction in zebrafish and its attenuation by L-arginine. Oncotarget. 2017;8: 58264–58271.
78. Dey A, Prabhudesai S, Zhang Y, Rao G, Thirugnanam K, Hossen MN, et al. Cystathione β-synthase regulates HIF-1α stability through persulfidation of PHD2. Sci Adv. 2020;6. doi:10.1126/sciadv.aaz8534
79. Ishii I, Akahoshi N, Yamada H, Nakano S, Izumi T, Suematsu M. Cystathionine gamma-Lyase-deficient mice require dietary cysteine to protect against acute lethal myopathy and oxidative injury. J Biol Chem. 2010;285: 26358–26368.
80. Heo Y-A. Sodium Phenylbutyrate and Ursodoxicoltaurine: First Approval. CNS Drugs. 2022;36: 1007–1013.
81. Huang K, Deng R, Liu T-C, Gremida A, Deepak P, Chen C-H, et al. A TRANSLATIONAL PHASE I STUDY OF TAUROURSODEOXYCHOLIC ACID (TUDCA) TO REDUCE SYMPTOMS AND ER STRESS IN ACTIVE ULCERATIVE COLITIS. Inflamm Bowel Dis. 2021;27: S5–S6.
82. Stroka KM, Vaitkus JA, Aranda-Espinoza H. Endothelial cells undergo morphological, biomechanical, and dynamic changes in response to tumor necrosis factor-α. Eur Biophys J. 2012;41: 939–947.
83. Urra H, Henriquez DR, Cánovas J, Villarroel-Campos D, Carreras-Sureda A, Pulgar E, et al. IRE1α governs cytoskeleton remodelling and cell migration through a direct interaction with filamin A. Nat Cell Biol. 2018;20: 942–953.
84. Pasini S, Liu J, Corona C, Peze-Heidsieck E, Shelanski M, Greene LA. Activating Transcription Factor 4 (ATF4) modulates Rho GTPase levels and function via regulation of RhoGDIα. Sci Rep. 2016;6: 36952.
85. Zhu J, Thompson CB. Metabolic regulation of cell growth and proliferation. Nat Rev Mol Cell Biol. 2019;20: 436–450.
86. Missiaen R, Morales-Rodriguez F, Eelen G, Carmeliet P. Targeting endothelial metabolism for anti-angiogenesis therapy: A pharmacological perspective. Vascul Pharmacol. 2017;90: 8–18.
87. Potente M, Carmeliet P. The Link Between Angiogenesis and Endothelial Metabolism. Annu Rev Physiol. 2017;79: 43–66.
88. Annunziata I, Sano R, d'Azzo A. Mitochondria-associated ER membranes (MAMs) and lysosomal storage diseases. Cell Death Dis. 2018;9: 1–16.
89. Inigo M, Deja S, Burgess SC. Ins and Outs of the TCA Cycle: The Central Role of Anaplerosis. Annu Rev Nutr. 2021;41: 19–47.

90. Timkova V, Tatarkova Z, Lehotsky J, Racay P, Dobrota D, Kaplan P. Effects of mild hyperhomocysteinemia on electron transport chain complexes, oxidative stress, and protein expression in rat cardiac mitochondria. Mol Cell Biochem. 2016;411: 261–270.
91. Merchan JR, Kovács K, Railsback JW, Kurtoglu M, Jing Y, Piña Y, et al. Antiangiogenic activity of 2-deoxy-D-glucose. PLoS One. 2010;5: e13699.
92. Gimbrone MA Jr, García-Cardeña G. Endothelial Cell Dysfunction and the Pathobiology of Atherosclerosis. Circ Res. 2016;118: 620–636.